A pharmacologically-based multiscale mathematical model of angiogenesis and its use in investigating the efficacy of a new cancer treatment strategy

Frédérique Billy[a], Benjamin Ribba[*,b,c], Olivier Saut[d], Hélène Morre-Trouilhet[a], Thierry Colin[d], Didier Bresch[b,f], Jean-Pierre Boissel[a], Emmanuel Grenier[e], Jean-Pierre Flandrois[a]

[a]*Université de Lyon, F-69000, Lyon; Université Lyon 1; CNRS, UMR5558, Laboratoire de Biométrie et Biologie Evolutive, F-69622, Villeurbanne, France.*
[b]*INRIA Grenoble Rhône-Alpes, 655 avenue de l'Europe, Montbonnot, F-38334 Saint Ismier Cedex, France.*
[c]*Université de Lyon, Lyon, F-69003, France; Université Lyon 1, EA3738 CTO, faculté de médecine Lyon-Sud, F-69600, Oullins, France.*
[d]*Université Bordeaux 1, Institut de Mathématiques de Bordeaux, CNRS, UMR5251 and INRIA Bordeaux Sud-Ouest EPI MC2, 351 cours de la libération, F-33405, Talence Cedex, France.*
[e]*Université de Lyon, Lyon, F-69003, France; ENS Lyon, Unité de Mathématiques Pures et Appliquées, CNRS, UMR5669, 46 allée d'Italie, F-69364, Lyon Cedex, France.*
[f]*Université de Savoie, Laboratoire de Mathématiques, CNRS, UMR5127, Campus Scientifique, F-73376, Le Bourget-du-Lac Cedex, France.*

Abstract

Tumor angiogenesis is the process by which new blood vessels are formed and enhance the oxygenation and growth of tumors. As angiogenesis is recognized as being a critical event in cancer development, considerable efforts have been made to identify inhibitors of this process. Cytostatic treatments that target the molecular events of the angiogenesis process have been developed, and have met with some success. However, it is usually difficult to preclinically assess the effectiveness of targeted therapies, and apparently promising compounds sometimes fail in clinical trials.

We have developed a multiscale mathematical model of angiogenesis and tumor growth. At the molecular level, the model focuses on molecular competition between pro- and anti-angiogenic substances modeled on the basis of pharmacological laws. At the tissue scale, the model uses partial differential equations to describe the spatio-temporal changes in cancer cells during three stages of the cell cycle, as well as those of the endothelial cells that constitute the blood vessel walls.

---

[*]Corresponding author: Tel: +33 4 26 23 59 63; Fax: +33 4 26 23 59 76

Email addresses: billy@biomserv.univ-lyon1.fr (Frédérique Billy), benjamin.ribba@inrialpes.fr (Benjamin Ribba), olivier.saut@math.u-bordeaux1.fr (Olivier Saut), helene.trouilhet@gmail.com (Hélène Morre-Trouilhet), colin@math.u-bordeaux1.fr (Thierry Colin), didier.bresch@univ-savoie.fr (Didier Bresch), jpb@upcl.univ-lyon1.fr (Jean-Pierre Boissel), emmanuel.grenier@umpa.ens-lyon.fr (Emmanuel Grenier), flandrs@biomserv.univ-lyon1.fr (Jean-Pierre Flandrois)

This model is used to qualitatively assess how efficient endostatin gene therapy is. Endostatin is an anti-angiogenic endogenous substance. The gene therapy entails overexpressing endostatin in the tumor and in the surrounding tissue. Simulations show that there is a critical treatment dose below which increasing the duration of treatment leads to a loss of efficacy.

This theoretical model may be useful to evaluate the efficacy of therapies targeting angiogenesis, and could therefore contribute to designing prospective clinical trials.

1. Introduction

Tumor angiogenesis is a process by which new blood vessels are formed from the existing vasculature and carry additional nutrients and oxygen to tumor cells, allowing them to proliferate. The development of the primary tumor mass and the metastatic dissemination of tumor cells require angiogenesis. It is generally accepted that a tumor, which needs nutrients and oxygen to grow, cannot increase beyond a few millimeters cubed without an enhanced blood supply (Folkman, 1990). During tumor growth, a molecular cascade drives the transition from the avascular stage to the vascular stage: new vessels are formed from the surrounding existing vasculature, migrate towards the tumor cells, and penetrate the tumor mass to deliver oxygen and nutrients to the tumor cells. This also means that some tumor cells can escape from this primary tumor, and enter the bloodstream via the newly formed immature and permeable blood vessels to form new tumor masses, also known as metastases, at distant parts of the body (Zetter, 1998; Folkman, 2002). In most cases, the presence of metastases is correlated with the malignancy of the tumor, and indicates a poor prognosis for the patient (Zetter, 1998).

Indeed, angiogenesis, or new vessel formation, results from a complex molecular balance between numerous pro-angiogenic and anti-angiogenic endogenous substances (Hanahan and Folkman, 1996).

2

The complexity of angiogenesis is partly due to the existence of a number of such factors. In breast cancer for instance, up to seven distinct pro-angiogenic factors can be expressed (Relf et al., 1997).

Over the last 25 years, several mathematical models of angiogenesis have been developed (see (Mantzaris et al., 2004) for a review). Discrete mathematical models, based on cellular automata, have usually been used to predict the structure of extra- and intra-tumoral vascular networks. Anderson and Chaplain have published the first discrete model of tumor-induced angiogenesis. This model was derived from a continuous model (Anderson and Chaplain, 1998). Several more recent publications are based on the same approach (Plank et al., 2004; Kevrekidis et al., 2006). Continuous models of tumor-induced angiogenesis are based on ordinary or partial differential equations governing the change in endothelial cell density, and the concentrations of tumor pro-angiogenic factors and of fibronectin (a component of the extracellular matrix). From the physical point of view, these models focus mainly on the endothelial cell diffusion, chemotaxis and haptotaxis (Anderson and Chaplain, 1998; Kevrekidis et al., 2006). It has also been proposed that mathematical models of angiogenesis can be coupled with those of tumor growth. In (Zheng et al., 2005), the authors have proposed a vascular tumor growth model in which the tumor growth model proposed by Byrne and Chaplain (Byrne and Chaplain, 1996) is coupled with a continuous-discrete model of angiogenesis, such as that described by Anderson and Chaplain in (Anderson and Chaplain, 1998). In (Hogea et al., 2006), the authors have coupled a model of tumor growth with a simplistic continuous model of angiogenesis. Several models of vascular tumor growth also include some mechanical constraints, such as wall shear stress, pressure. For instance, in (Alarcón et al., 2005), Alarcón and colleagues have coupled a cellular automaton with ordinary differential equations (ODEs) to describe some of the interactions that occur between the tissue scale, including vascular structural adaptation, the cellular scale and the intracellular scale. In (Bartha and Rieger, 2006; Lee et al., 2006; Welter et al., 2008), the authors have used models based on probabilistic cellular automata to investigate the mechanisms leading to abnormal tumor vasculature, and the effects of such vascular heterogeneities on tumor growth and drug delivery. In order to circumvent the numerical cost of such cellular automata, Macklin and colleagues (Macklin et al., 2009) have decided to combine a continuous model of tumor growth with a discrete model of tumor-induced angiogenesis, such as that described by McDougall and colleagues in (McDougall et al., 2006). Thanks to this combination, they were able to take into account the impact of blood flow on changes in the vascular

3

network. Due to their complexity, these models are only qualitative, and even so can only integrate one or two of the molecular factors that drive the angiogenesis process. Moreover, the underlying tumor growth model is often very simplistic and fails to take cell cycle regulation into account.

Since the angiogenic process was first identified as a key process in tumor development a few years ago, pharmaceutical companies have been looking for inhibitors. Several anti-angiogenic molecules have been identified and tested in clinical trials but, as is all too often the case with targeted therapies, efficacy has been difficult to demonstrate. This makes it rather difficult to assess attempts to optimize treatment. New anti-cancer drugs are designed to target a particular cancer process, unlike standard chemotherapeutic compounds that have a cytotoxic effect on all proliferative cells. Targeted therapies, which are also known as "cytostatic treatments", act mainly at the molecular level. For instance, some anti-angiogenic drugs, the best known being Bevacizumab (Avastin, Roche), prevent vascular endothelial growth factor (VEGF), a pro-angiogenic endogenous substance, from binding to Flk-1 receptors. These receptors are located on the membrane of endothelial cells, which constitute blood vessels. Such anti-angiogenic drugs inhibit endothelial cell proliferation and, in consequence, prevent new blood vessels from forming, without any direct toxic effect on healthy cells.

To make it possible to analyze the effect of such molecular-targeted treatments by means of mathematical models, we need to include the main molecular entities in multiscale models of tumor growth. In this paper we describe a pharmacologically-based continuous mathematical model of angiogenesis and tumor growth. At the molecular level, we were careful to use pharmacological laws to model the activation of angiogenesis as the result of the binding of major angiogenic molecular substances to their respective receptors. This molecular-level model was embedded in the macroscopic model, based on reaction-diffusion partial differential equations, which described the spatio-temporal change in the densities of the unstable and stable endothelial cells that constitute the blood vessel wall. At each of the time steps in the model, sources of oxygen were defined according to the spatial disposition of the endothelial cells. The oxygen concentration was then computed, and introduced as an input signal into the cell cycle model of tumor cells. Indeed, depending on the local concentration of oxygen, we assumed that cancer cells would proliferate, die, or enter the quiescent compartment. In the model, quiescent cells, deprived of oxygen, secrete vascular endothelial growth factor (VEGF). This in turn activates angiogenesis, and this constitutes the feedback loop

4

of the model.

We applied our model to an analysis of the efficacy of a new anti-angiogenesis treatment. This treatment relies on the overproduction of an endogenous anti-angiogenic substance known as endostatin, which is commonly secreted by tumor cells (O'Reilly et al., 1997). Endostatin is a 20-kDa, C-terminal fragment of collagen XVIII, and has been shown to be a potent endogenous inhibitor of angiogenesis (O'Reilly et al., 1997). Endostatin gene therapy consists of infecting tumor cells with adenoviruses encoding a wild-type endostatin gene (Folkman, 2006). When feasible, these adenoviruses are injected directly into the tumor mass, which induces targeted local overexpression of endostatin. This approach is currently being evaluated in clinical trials (Lin et al., 2007; Li et al., 2008). However, as is often the case for targeted anti-cancer therapies, it is hard to identify the best treatment strategy.

Using the multiscale model of tumor growth and angiogenesis to carry out a qualitative analysis of the effect of this treatment, we provide some indications about the best way to optimize this cancer treatment strategy.

2. Underlying biological hypotheses and an overall view of the mathematical model

Due to the complexity of the problem, we first collected biological information from the literature, and made some simplified hypotheses about the various biological phenomena involved. The diagram shown in Figure 1 was developed in collaboration with biologists. It provides a schematic description of the relationships between the different entities we will model in this study.

Our model includes two main species of cells. The first is that of the endothelial cells that constitute the wall of blood vessels. We distinguished between unstable and stable endothelial cells, and assumed that only stable endothelial cells could constitute a source of oxygen supply for the tumor. As we discuss below, our approach was a continuous one. This means that we were not
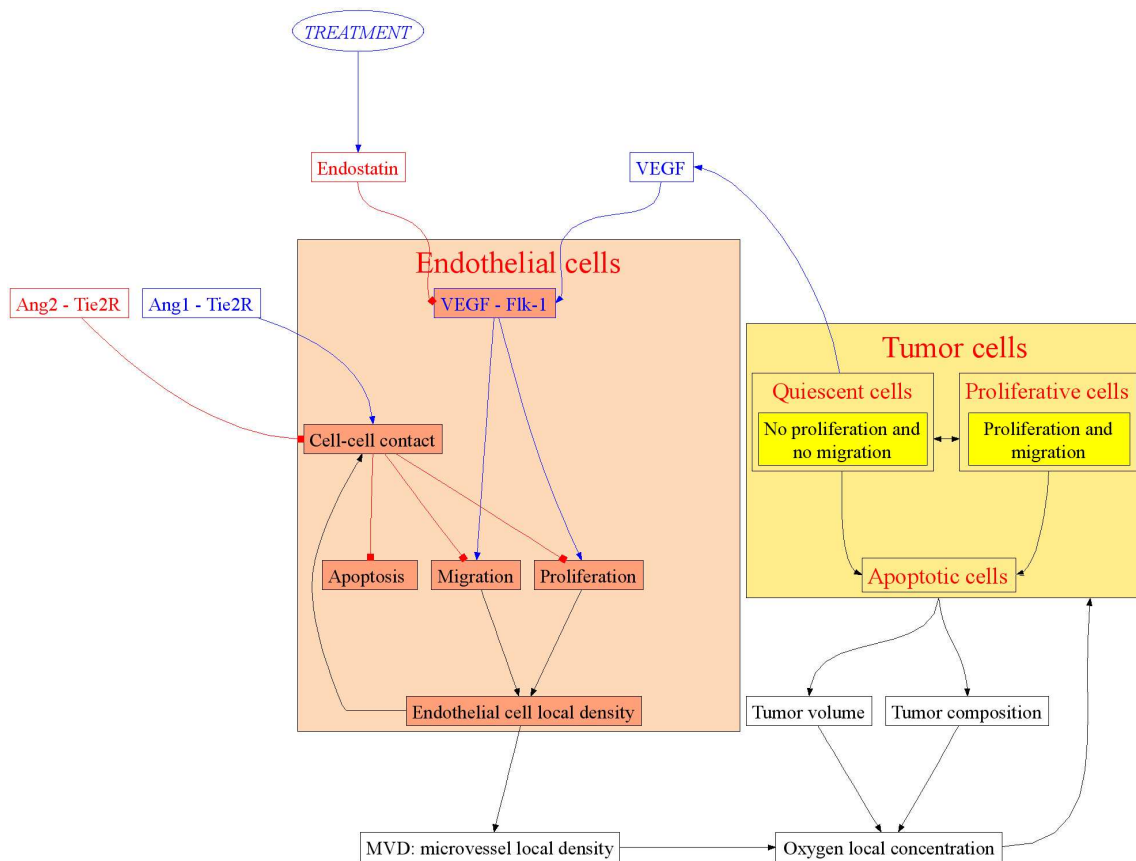
Figure 1: Summary of the biological entities and interactions taken into account in our mathematical model. The actions of activating substances (VEGF, angiopoietin-1 (Ang1)) are depicted by blue arrows, whereas those of inhibitors (endostatin, angiopoietin-2 (Ang2)) are depicted by red arrows. We distinguished between two species of cells: endothelial cells (unstable and stable), and tumor cells (proliferative, quiescent or hypoxic, and apoptotic). Quiescent tumor cells secrete VEGF molecules that stimulate the proliferation of endothelial cells and their migration towards tumor cells. Moreover, competition between angiopoietin-1 and angiopoietin-2 regulates the stabilization of endothelial cells and, consequently, the maturation of the newly-formed blood vessels. These new vessels increase the supply of oxygen to the tumor cells. Finally, we modeled the action of a treatment leading to endostatin overproduction that, as we shall see in this papier, modifies the entire process of tumor growth and angiogenesis.

modeling blood vessels as discrete objects, but rather as continuous densities of endothelial cells that potentially constitute sources of oxygen. As we describe below, the regulation of stable and unstable endothelial cells results from molecular competition between activators and inhibitors of

angiogenesis.

The second type of cells we took into account was cancer cells. In our model, we distinguished between three types of cancer cells: proliferative, quiescent and apoptotic cells. Transitions between these states are mainly governed by the local concentration of oxygen.

We use the word "apoptosis" to refer to cell death of all kinds.

2.1. Model of tumor growth

Our mathematical model of tumor growth is based on a published age-structured model of the cell cycle applied to investigating the therapeutic benefits of various cancer treatment strategies (Ribba et al., 2006a,b, 2009). In our model, tumor cells can be in three different states: proliferative, quiescent, and apoptotic. Proliferative cells progress through the cell cycle, and duplicate. However, if the oxygen concentration is not sufficient for the cells to proliferate, the cells become quiescent (or hypoxic) cells. In this state, cells are assumed to secrete vascular endothelial growth factor (VEGF), an activator of angiogenesis, that diffuses into the surrounding tissue until it reaches the endothelial cells (Ferrara, 2002). If the environmental conditions become more favorable, these quiescent cells can revert to the proliferative state. However, if the oxygen concentration falls below a critical threshold, acute hypoxia will lead to cell apoptosis (Blagosklonny and Pardee, 2002; DeVita et al., 2005). At this stage, we made no attempt to take into account the biomechanical aspects of tumor growth. This hypothesis is discussed in detail in the Discussion section of this paper.

This model therefore consists of a multiscale framework, combining a hypoxia-driven cell cycle regulation model and a macroscopic spatial tumor growth model, in which cell populations are modeled as a multiphase fluid governed by Darcy's law. The output from the cell cycle model is the net proliferation rate of the entire cell population. This information is used at the macroscopic level to compute the motion of tumor cells in the computational domain. The spatial locations of the density of stable endothelial cells are calculated thanks to the macroscopic level of the model. These locations constitute new oxygen sources, and so are used to compute the field of oxygen. This field of oxygen becomes the input signal for the cell cycle model, which computes the densities of proliferative, hypoxic and apoptotic cells, depending on the oxygen available to tumor cells (see Figure 2).
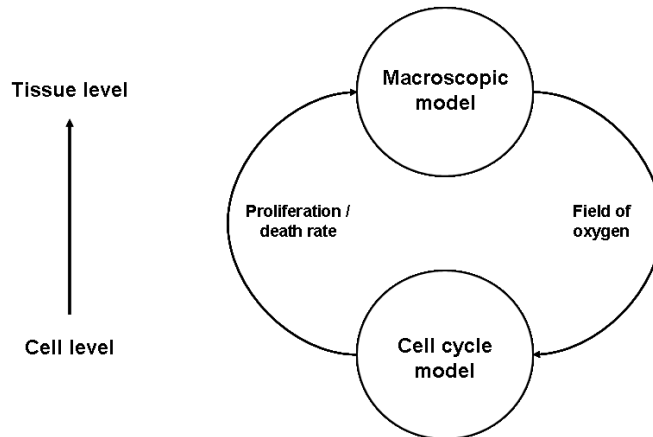
7

Figure 2: Multiscale aspect of the model (inspired of (Ribba et al., 2009)). The motion of tumor cells in the computational domain is computed at the macroscopic level, resulting, through the angiogenesis process, in new sources of oxygen. Thus, the new field of oxygen becomes the input signal of the cell cycle model, which computes the density of proliferative, hypoxic and apoptotic cells.

2.2. Model of angiogenesis

Our angiogenesis model focuses on the spatio-temporal change in the density of endothelial cells. As we have already said, we distinguished between unstable and stable endothelial cells. Unstable endothelial cells naturally undergo random diffusion. They proliferate in response to the stimulus of the VEGF molecules secreted by hypoxic tumor cells. At the molecular level, we used conventional pharmacological laws to model the binding of VEGF to Flk-1 receptors (also known as KDR or VEGFR-2) on the membranes of the unstable endothelial cells (Ferrara, 1999a, 2002). However, VEGF stimulation is modulated by the antagonist endostatin, which is also produced by tumor cells, and which competes with VEGF to bind to Flk-1 receptors (Kim et al., 2002). VEGF-stimulated unstable endothelial cells therefore proliferate and migrate along the gradient of VEGF concentration, i.e. towards the hypoxic cell population (Ausprunk and Folkman, 1977; Paweletz and Knierim, 1989; Ferrara, 1999b). At this stage, we ignored that endothelial cells and extracellular matrix could interact during the process of migration, and could lead to the haptotactic motion. This motion has been modeled in several papers (Anderson and Chaplain, 1998; Zheng et al., 2005; Macklin et al., 2009; McDougall et al., 2006). Non-stimulated, unstable endothelial cells do not proliferate, and eventually die (Benjamin and Keshet, 1997; Ferrara, 1999b).

8

We assumed, though without modeling this, that unstable cells instantaneously form immature tubular structures that are a prerequisite for the appearance of mature blood vessels able to carry oxygen. In our model, the transition from unstable to stable endothelial cells leads the immature vessels to turn into mature and functional blood vessels. This transition is mediated by cell-to-cell contact, regulated through the competitive binding of angiopoietin-1 and angiopoietin-2 to Tie2 receptors located on the membrane of unstable endothelial cells (Partanen et al., 1992). Angiopoietin-1 is expressed by mural cells, which play an important role in the maturation of new blood vessels (Sundberg et al., 2002). Angiopoietin-2 is produced both by tumor cells and by unstable endothelial cells (Etoh et al., 2001; Ahmad et al., 2001; Koga et al., 2001; Tanaka et al., 2002; Moon et al., 2003; Hu et al., 2003). Angiopoietin-1 is known to promote contact between endothelial cells, whereas angiopoietin-2 blocks the activation of Tie2 by angiopoietin-1 (Davis et al., 1996; Maisonpierre et al., 1997). In our model, when the contact between endothelial cells reaches a sufficient level, proliferation, migration and apoptosis stop, and unstable endothelial cells revert to being stable cells. As we have already pointed out, the presence of stable endothelial cells is a prerequisite for the appearance of functional blood vessels able to carry oxygen to the tumor cells. In our model, we simply assumed that unless the density of stable endothelial cells was zero, a microscopic source would diffuse oxygen into the surrounding tissue. This oxygen would then be consumed by tumor cells. Finally, we assumed that the tumor mass could disrupt the behavior of unstable endothelial cells, but, at this stage, we did not take into account its possible impact on the behavior of the whole vascular network.

In conclusion, we adopted a somewhat phenomenological approach to modeling the angiogenesis process. This is inherent to the continuous approach we chose to use. However, we claim that it suffices to qualitatively study how efficient innovative anti-angiogenic treatments are. We will return to this topic in the Discussion section of this paper.

2.3. Endostatin-based treatment model

Endostatin-based cancer treatment involves enhancing the concentration of the angiogenesis inhibitor endostatin in order to reduce the binding of VEGF to Flk-1 receptors and, consequently, to

reduce the activation of unstable endothelial cells. Endostatin has been shown to promote blood vessel regression (O'Reilly et al., 1997; Folkman, 2006; Kim et al., 2002; Sauter et al., 2000).

In this paper, we are interested in an endostatin gene therapy that involves the local infection of tumor cells with adenoviruses encoding the wild-type endostatin gene. This results in the overproduction of endostatin by the cancer cells. As we were intending to carry out a qualitative analysis of the efficacy of this treatment strategy, we modeled the administration of the adenoviruses rather simply. We assumed that the adenovirus particles had been rendered replication-deficient (Lin et al., 2007), and that this would homogeneously induce the overproduction of endostatin by quiescent and proliferative tumor cells. We also assumed that the diffusion of the adenoviruses outside the tumor could be neglected, and so we did not take into account their possible impact on endothelial and other healthy cells, assuming that it would be negligible compared to their effect on the tumor cells.

In what follows, we studied the effectiveness of a single administration of adenoviruses to avoid the issue of a possible immune response, that can occur following the first administration of treatment, and could therefore modify the efficacy of subsequent administrations.

3. Equations of the mathematical model

Our virtual tumor is described by the densities of tumor cells (number of tumor cells per unit of volume) in the proliferative, quiescent and apoptotic phases.

Newly-formed blood vessels are represented by the density of endothelial cells (continuous approach), with a distinction being made between stable and unstable cells. Unstable cells proliferate and migrate towards the source of VEGF, whereas stable cells, which are required for blood to flow, are static.

We modeled the tissue concentrations of the biochemical substances investigated (VEGF, endostatin, angiopoietin-1 and angiopoietin-2) and oxygen.

Our model is based on a set of reaction-diffusion partial differential equations, that describes the evolution of the densities and concentrations of the species we took into account. The interaction between these species and regulation rules are described by a non-linear dependence of the coefficients of the equations.

Table 1 summarizes the notations used in this section.

Variable	Description
Ω	Computation domain
n	Density of unstable endothelial cells
n_S	Density of stable endothelial cells
$[VEGF]$	VEGF concentration
$[endos]$	Endostatin concentration
$[Ang1]$	Angiopoietin-1 concentration
$[Ang2]$	Angiopoietin-2 concentration
$[O_2]$	Oxygen concentration
P	Density of proliferative tumor cells
Q	Density of quiescent tumor cells
A	Density of apoptotic tumor cells
M	Density of healthy cells

Table 1: Notations used in the mathematical model.

All variables (local densities and concentrations) are assumed to be functions of space (denoted by $\mathbf{x}$), and time (denoted by t). To simplify, we will omit symbols indicating time and space dependencies, and will write, for instance, n instead of $n(\mathbf{x}, t)$.

3.1. Densities of endothelial cells

As we have already explained, unstable endothelial cells undergo four processes: proliferation (until a maximum value denoted by N_{max} is reached), diffusion, chemotaxis in response to VEGF stimuli and depending on the VEGF concentration gradient, and maturation.

Consequently, at the space position $\mathbf{x}$ and time t, the density of unstable endothelial cells is governed by:

$$\frac{\partial n}{\partial t} = \underbrace{\nabla \cdot (D_e \, \nabla n)}_{diffusion} + \underbrace{\alpha \, n \, \left(1 - \frac{n + n_S}{N_{max}}\right)}_{proliferation} - \underbrace{\nabla \cdot \left(\chi \, n \, \left(1 - \frac{n + n_S}{N_{max}}\right) \, \nabla[VEGF]\right)}_{chemotaxis} - \underbrace{\frac{\partial n_S}{\partial t}}_{maturation} \quad (1)$$

where D_e is the diffusion coefficient, α the proliferation rate, χ the chemotaxis rate. (See equation (2) for details about $\frac{\partial n_S}{\partial t}$.)

Thus, we modeled the proliferation of unstable endothelial cells using a logistic-type growth model, incorporating a logistic-type inhibition function to describe the fact that the number of endothelial cells cannot exceed the maximum value N_{max} (due to tissue carrying capacities, for instance). This inhibition function was also introduced into the chemotaxis term to model the natural affinity of endothelial cells for one another: the higher the local density of these cells, the fewer endothelial cells move away. Moreover, we assumed that the diffusion of unstable endothelial cells would be sharply reduced in places where the tumor density was too high, as a result of pressure effects and lack of space. To simplify, the diffusion coefficient, D_e, was taken to be usually constant, equal to C_e, but to be multiplied by a constant $c_{e,d} < 1$ in places where the tumor density $(P+Q)$ was above a given threshold $\tau_{e,d}$, so we get:

$$\forall t, \; \forall \mathbf{x} \in \Omega \qquad D_e(\mathbf{x}, t) = C_e * \lambda_{e,d}(\mathbf{x}, t)$$

where

$$\lambda_{e,d}(\mathbf{x}, t) = \begin{cases} c_{e,d} < 1 & if \; P(\mathbf{x}, t) + Q(\mathbf{x}, t) > \tau_{e,d} \\ 1 & else \end{cases}$$

(see section 3.6 for details about P and Q)

We assumed that the proliferation and migration rates (α and χ respectively in equation (1)) depended on the biochemical species effects on endothelial cells. So, in our model, α and χ depend on VEGF (see below).

12

Effect of VEGF on the proliferation of unstable endothelial cells. VEGF promotes the proliferation of endothelial cells by binding to Flk-1 receptors. However, this binding is regulated by endostatin, which is a VEGF antagonist at these receptors. This means that the effect of VEGF is regulated by endostatin. To model the effect of VEGF on the proliferation of unstable endothelial cells (denoted by $E_{VEGF,prolif}$) in the presence of endostatin, we used the standard pharmacological *Emax* model in order to take into account the differences between the molecular properties of VEGF and endostatin (see Appendix A for details):

$$E_{VEGF,prolif} = \frac{Emax_{VEGF,prolif}}{1 + \frac{K_{D,VEGF}}{[VEGF]}\left(1 + \frac{[endos]}{K_{D,endos}}\right)}$$

where $Emax_{VEGF,prolif}$ denotes the maximum effect of VEGF on unstable endothelial cell proliferation, and $K_{D,VEGF}$ (resp. $K_{D,endos}$) the dissociation constant of VEGF (resp. endostatin) at its Flk-1 receptor.

As expected, according to the previous equation, increasing the endostatin concentration induces a decrease in the effect of VEGF on proliferation.

However, unstable endothelial cells are known to die if the proliferation rate is not high enough. Consequently, the proliferation rate becomes negative if $E_{VEGF,prolif}$ is below a given threshold (denoted by $Emin_{prolif}$). We modeled this condition using the PA function defined below:

$$PA(u) = (\frac{Ap + u}{2}) - (\frac{Ap - u}{2})\, tanh(10^2(u - Emin_{prolif})) \quad \forall u \geq 0$$

where $Emin_{prolif}$ is the minimum value of $E_{VEGF,prolif}$, below which the proliferation rate becomes negative (value Ap).

As for the diffusion process, we assumed that endothelial cells would proliferate less in places where tumor density was too high, because of pressure effects and lack of space. So we assumed the proliferation rate to be multiplied by a given constant $c_{e,p} < 1$ in places where tumor density was above a given threshold $\tau_{e,p}$. This was equivalent to multiplying the proliferation rate by $\lambda_{e,p}$ defined as follows:

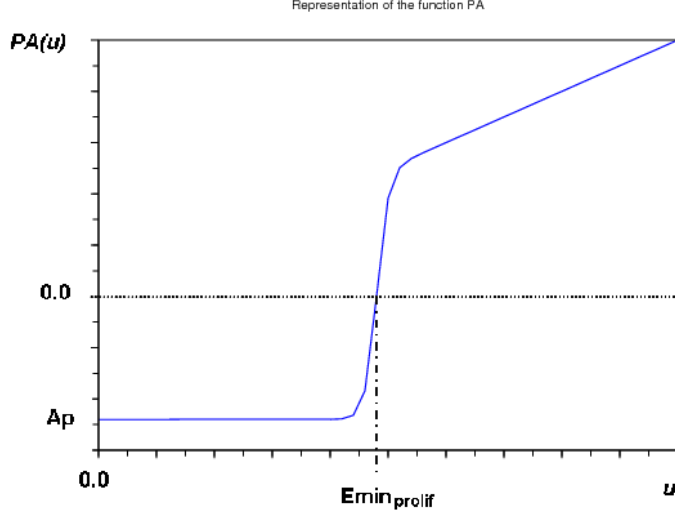$$\lambda_{e,p} = \begin{cases} c_{e,p} < 1 & if \ P + Q > \tau_{e,p} \\ 1 & else \end{cases}$$

13

Figure 3: Representation of the PA function. $Emin_{prolif}$ corresponds the minimum value of $E_{VEGF,prolif}$, below which cellular proliferation no longer occurs; Ap is a negative constant representing the cell death rate.

The proliferation rate is finally given by the following expression:

$$\alpha = PA(E_{VEGF,prolif})\,\lambda_{e,p}$$

Effect of VEGF on the chemotaxis of unstable endothelial cells. We assumed that the chemotactic rate χ depended on VEGF binding to Flk-1 receptors. Using the *Emax* model, as before, we obtained:

$$\chi = \lambda_{e,c}\,\frac{Emax_{VEGF,chemo}}{1 + \dfrac{K_{D,VEGF}}{[VEGF]}\left(1 + \dfrac{[endos]}{K_{D,endos}}\right)}$$

where $Emax_{VEGF,chemo}$ denotes the maximum effect of VEGF on unstable endothelial cell chemotaxis, and $K_{D,VEGF}$ (resp. $K_{D,endos}$) the dissociation constant of VEGF (resp. endostatin) at its Flk-1 receptor.

14

As before, we multiplied the chemotactic coefficient by a constant $c_{e,c} < 1$, where the tumor density was above a given threshold $\tau_{e,c}$:

$$\lambda_{e,c} = \begin{cases} c_{e,c} < 1 & if\ P + Q > \tau_{e,c} \\ 1 & else \end{cases}$$

Moreover, in our model, unstable endothelial cells become stable through the maturation process. This maturation process depends on the effects of angiopoietins as they bind to the Tie2 receptors.

Effect of angiopoietins on endothelial cell maturation. As before, the pharmacological *Emax* model was used to model the combined impact of angiopoietin-1 and its antagonist, angiopoietin-2, on the maturation of unstable endothelial cells:

$$E_{Ang1} = \frac{Emax_{Ang1}}{1 + \dfrac{K_{D,Ang1}}{[Ang1]}\left(1 + \dfrac{[Ang2]}{K_{D,Ang2}}\right)}$$

where $Emax_{Ang1}$ represents the maximum effect of angiopoietin-1 on unstable endothelial cells, and $K_{D,Ang1}$ (resp. $K_{D,Ang2}$) the dissociation constant of angiopoietin-1 (resp. -2) at the Tie2 receptor.

We also assumed that endothelial cells matured when E_{Ang1} was above a given threshold $E_{Ang1_{min}}$. In consequence, the evolution of the density of stable (mature) endothelial cells is given by the following expression:

$$\frac{\partial n_S}{\partial t} = \mu\, H(E_{Ang1} - E_{Ang1_{min}})\, H(n + n_S - N_{min})\, n \tag{2}$$

where μ denotes the maturation rate, H the Heaviside function, $E_{Ang1_{min}}$ and N_{min} are the minimum value of E_{Ang1} and that of endothelial cell density required for maturation, respectively. We assumed μ, $E_{Ang1_{min}}$ and N_{min} to be positive constants.

3.2. VEGF concentration

VEGF is secreted by quiescent tumor cells, diffuses into the surrounding tissue, binds to specific receptors located on endothelial cell membranes, and disappears naturally. As in the foregoing

tumor modeling framework, we assumed that the process of molecular diffusion occurred on a much shorter time scale than that of cell division (Ribba et al., 2005). Therefore, in our model, the VEGF concentration reaches steady-state instantaneously, and so is supposed to satisfy the following equation:

$$0 = \frac{\partial [VEGF]}{\partial t} = \underbrace{\nabla \cdot (D_V \, \nabla [VEGF])}_{diffusion} + \underbrace{\alpha_V \, Q}_{production} - \underbrace{\beta_V \, n}_{binding} - \underbrace{\delta_V \, [VEGF]}_{natural \; decay} \qquad (3)$$

where D_V is the diffusion coefficient, α_V the production rate, β_V the binding rate, δ_V the degradation rate. D_V, α_V and δ_V are taken to be positive constants.

As we said before, endostatin is a competitive inhibitor of VEGF at the Flk-1 receptors. We therefore modeled the binding rate of VEGF to its receptors as follows:

$$\beta_V = \frac{\beta_{max,V}}{1 + \dfrac{K_{D,VEGF}}{[VEGF]} \left(1 + \dfrac{[endos]}{K_{D,endos}} \right)}$$

where $\beta_{max,V}$ denotes the maximum binding rate of VEGF to Flk-1 receptors, $K_{D,VEGF}$ (resp. $K_{D,endos}$) is the dissociation constant of VEGF (resp. endostatin) at its Flk-1 receptor. These three parameters are all positive constants.

3.3. Endostatin concentration

Endostatin is released by living tumor cells (proliferative and quiescent), diffuses into the surrounding tissue, binds to specific Flk-1 receptors, and disappears naturally. As for VEGF, we assumed that the endostatin concentration also reached steady-state instantaneously. The endostatin concentration therefore satisfies the following equation:

$$0 = \frac{\partial [endos]}{\partial t} = \underbrace{\nabla \cdot (D_{endos} \, \nabla [endos])}_{diffusion} + \underbrace{\alpha_{endos} \, (P + Q)}_{production} - \underbrace{\beta_{endos} \, n}_{binding} - \underbrace{\delta_{endos} \, [endos]}_{natural \; decay} \qquad (4)$$

where D_{endos} is the diffusion coefficient, α_{endos} the production rate, β_{endos} the binding rate, δ_{endos} the degradation rate. D_{endos}, α_{endos} and δ_{endos} are positive constants.

16

As VEGF and endostatin are competitive inhibitors, the binding rate of endostatin to its Flk-1 receptors is modeled by:

$$\beta_{endos} = \frac{\beta_{max,endos}}{1 + \frac{K_{D,endos}}{[endos]}\left(1 + \frac{[VEGF]}{K_{D,VEGF}}\right)}$$

where $\beta_{max,endos}$ denotes the maximum binding rate of endostatin to Flk-1 receptors, $K_{D,endos}$ (resp. $K_{D,VEGF}$) is the dissociation constant of endostatin (resp. VEGF) at its Flk-1 receptor. As before, these three parameters are all positive constants.

3.4. Concentrations of the angiopoietins

As we said above, angiopoietin-1 is expressed by mural cells, which play an important role in the maturation process of new blood vessels. As our model does not integrate mural cells, we will assume the angiopoietin-1 concentration to be uniformly constant (equal to $[Ang1]_0$), which seems a plausible hypothesis (Metheny-Barlow and Li, 2003).

Angiopoietin-2 is produced by tumor cells and by unstable endothelial cells, and it diffuses into the surrounding tissue, binds to specific receptors Tie2, and disappears naturally. Making the same assumptions as for the VEGF equation, we can write:

$$0 = \frac{\partial[Ang2]}{\partial t} = \underbrace{\nabla \cdot (D_{A2}\,\nabla[Ang2])}_{diffusion} + \underbrace{\alpha_{1,A2}\,(P+Q) + \alpha_{2,A2}\,n}_{production} - \underbrace{\beta_{A2}\,n}_{binding} - \underbrace{\delta_{A2}\,[Ang2]}_{natural\ decay} \qquad (5)$$

where D_{A2} stands for the diffusion coefficient, $\alpha_{1,A2}$ and $\alpha_{2,A2}$ the production rates, β_{A2} the binding rate, δ_{A2} the degradation rate. D_{A2}, $\alpha_{1,A2}$, $\alpha_{2,A2}$ and δ_{A2} are positive constants. As before, we expressed the binding rate of angiopoietin-2 to Tie2 receptors as follows:

$$\beta_{A2} = \frac{\beta_{max,A2}}{1 + \frac{K_{D,A2}}{[Ang2]}\left(1 + \frac{[Ang1]}{K_{D,A1}}\right)}$$

where $\beta_{max,A2}$ denotes the maximum binding rate, $K_{D,A2}$ (resp. $K_{D,A1}$) is the dissociation constant of angiopoietin-2 (resp. angiopoietin-1) at its Tie2 receptor.

17

3.5. Oxygen concentration

As we said above, the angiogenesis model is coupled to the tumor growth model by oxygen concentration.

Oxygen is delivered by the pre-existing vasculature and by the vessels newly-formed as a result of angiogenesis. We assumed that oxygen diffuses through the vessels wall into the surrounding tissue, is consumed by both healthy and tumor cells, and disappears naturally. We also assumed that the new sources of oxygen resulting from the angiogenic process had a constant concentration ($[O_2]_{max}$), and were located in those spaces where the density of stable endothelial cells was strictly positive (represented, for a given time t, by $\{\mathbf{x} \in \Omega \mid n_S(\mathbf{x}, t) \neq 0\}$).

Moreover, as before, we assumed that the oxygen concentration reached its steady-state instantaneously. Accepting these hypotheses, we wrote the equation governing the oxygen concentration as follows:

$$
\begin{cases}
0 = \dfrac{\partial [O_2]}{\partial t} = \underbrace{\nabla \cdot (D_O \, \nabla [O_2])}_{diffusion} - \underbrace{(\beta_{1,O} \, P + \beta_{2,O} \, Q + \beta_{3,O} \, M) \, [O_2]}_{consumption} - \underbrace{\delta_O \, [O_2]}_{natural \; decay} \\[2em]
[O_2] = [O_2]_{max} \text{ where } n_S \neq 0
\end{cases}
\tag{6}
$$

where D_O is the diffusion coefficient, $\beta_{1,O}$, $\beta_{2,O}$ and $\beta_{3,O}$ the consumption rates, δ_O the degradation rate. D_O, $\beta_{1,O}$, $\beta_{2,O}$ and $\beta_{3,O}$, δ_O and $[O_2]_{max}$ are all positive constants.

3.6. Densities of tumor cells and healthy cells

Our mathematical model of tumor growth, coupled with the angiogenesis model presented above, is based on a model published in several different papers (Ribba et al., 2006a,b, 2009). In our model, the tumor is described by the densities of tumor cells in the proliferative, quiescent, and apoptotic states.

The densities of tumor cells in these states are denoted by P_1, P_2 for the two proliferative phases, Q for the quiescent phase and A for apoptosis, respectively. This model takes into account the progression of tumor cells in the cell cycle by introducing the notion of age, denoted by a (age-structured model). However, we considered that only proliferative cells actually changed with age, so P_1 and P_2 depend on space $\mathbf{x}$, time t and age a, whereas Q and A only depend on space $\mathbf{x}$ and time t.

We then supposed the total proliferative cell density to be given by:

$$P(\mathbf{x},t) \overset{def}{=} \int_0^{a_{max,P_1}} P_1(\mathbf{x},t,a)\, da + \int_0^{a_{max,P_2}} P_2(\mathbf{x},t,a)\, da \quad \forall \mathbf{x} \in \Omega, \ \forall t$$

where a_{max,P_1} and a_{max,P_2} represent the maximum duration of the proliferative states represented by P_1 and P_2 respectively.

Cell division, leading to new cells, is assumed to create passive advection of tumor and healthy cells.

In our model, the transition between the proliferative (P_1) and the quiescent (Q) phases is governed by both hypoxia and overpopulation (when cells lack the space to proliferate), whereas the transition between the quiescent and apoptotic (A) phases is mediated solely by hypoxia. Figure 4 shows a schematic illustration of cell cycle regulation.
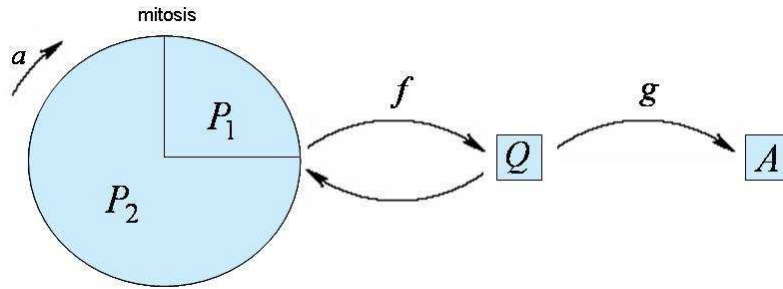

Figure 4: Schematic representation of our age-structured cell cycle regulation model. We took into account two proliferative phases P_1 and P_2, one quiescent phase Q, and one apoptotic phase A. At the end of the P_1 phase, environmental conditions are checked; this checking is modeled through functions f and g. In a context of overpopulation or hypoxia, proliferative cells become quiescent (through function f). If the hypoxic stress is too high, cells can become apoptotic (through function g). If the environmental conditions become more favorable, quiescent cells can revert to the proliferative phase. We suppose that mitosis occurs at the end of the P_2 phase, leading to the generation of new cells.

Functions f and g model the environmental conditions, with:

$$f(\mathbf{x}, t) = \begin{cases} 1 & if \ \int_0^{a_{max,P_1}} P_1(\mathbf{x}, t, a) \, da + 2 \int_0^{a_{max,P_2}} P_2(\mathbf{x}, t, a) \, da \\ & \qquad + Q(\mathbf{x}, t) \leq \tau_o \ \text{ and } \ [O_2](\mathbf{x}, t) \geq \tau_{1,h} \\ 0 & else \end{cases}$$

$$\text{and} \quad g(\mathbf{x}, t) = \begin{cases} 1 & if \ [O_2](\mathbf{x}, t) \geq \tau_{2,h} \\ 0 & else \end{cases}$$

where τ_o is the overpopulation threshold, and $\tau_{1,h}$ and $\tau_{2,h}$ the hypoxia thresholds (with $\tau_{1,h} > \tau_{2,h}$).

Let us note that we added a coefficient 2 before the P_2 density in the expression of the function f as cancer cells divide unconditionally once they are in the phase P_2.

The tumor cell density evolution equations are described below:

$$\frac{\partial P_1}{\partial t} + \frac{\partial P_1}{\partial a} + \nabla \cdot (\mathbf{v_{P_1}} \, P_1) = 0 \tag{7}$$

$$\frac{\partial P_2}{\partial t} + \frac{\partial P_2}{\partial a} + \nabla \cdot (\mathbf{v_{P_2}} \, P_2) = 0 \tag{8}$$

$$\frac{\partial Q}{\partial t} + \nabla \cdot (\mathbf{v_Q} \, Q) = g \, (1 - f) \, P_1(a = a_{max,P_1}) - \left[\frac{\partial f}{\partial t}\right]^+ Q(t^-) + \left[\frac{\partial g}{\partial t}\right]^- Q(t^-) \tag{9}$$

$$\frac{\partial A}{\partial t} + \nabla \cdot (\mathbf{v_A} \, A) = (1 - g) \, P_1(a = a_{max,P_1}) - \left[\frac{\partial g}{\partial t}\right]^- Q(t^-) \tag{10}$$

where $\left[\frac{\partial \, \cdot}{\partial t}\right]^+$ (resp. $\left[\frac{\partial \, \cdot}{\partial t}\right]^-$) represents the positive (resp. negative) part of $\frac{\partial \, \cdot}{\partial t}$, and $\mathbf{v_{P_1}}$, $\mathbf{v_{P_2}}$, $\mathbf{v_Q}$, $\mathbf{v_A}$ represent the velocity of tumor cells in the proliferative, quiescent and apoptotic states respectively. Since, as we said, the advection movement is passive, we assumed that $\mathbf{v_{P_1}} = \mathbf{v_{P_2}} = \mathbf{v_Q} = \mathbf{v_A}$, denoted by $\mathbf{v}$ in the following.

To model the transition between the two proliferative states, we supposed that the boundary conditions for age were given by:

$$\begin{cases} P_1(a = 0) = 2P_2(a = a_{max,P_2}) \\ P_2(a = 0) = fP_1(a = a_{max,P_1}) + \left[\frac{\partial f}{\partial t}\right]^+ Q(t^-) \end{cases} \tag{11}$$

20

Expansion of tumor cells induces a similar passive movement of healthy cells; so the density of healthy cells is assumed to be governed by:

$$\frac{\partial M}{\partial t} + \nabla \cdot (\mathbf{v_M}\, M) = 0 \tag{12}$$

where $\mathbf{v_M}$ represents the velocity of healthy cells, with $\mathbf{v_M} = \mathbf{v}$.

Note that, in our model, apoptotic cells (cells in phase A) do not disappear. Indeed, assuming the total density of cells (healthy cells plus tumor cells) to be equal to a constant, N_0, we set :

$$M + P + Q + A = N_0 \tag{13}$$

By deriving this equality with respect to time, we get:

$$\nabla \cdot \mathbf{v} = \frac{1}{N_0} P_2(a_{max,P_2}) \tag{14}$$

From this equation, we get $\nabla \cdot \mathbf{v} \geq 0$, which means that tumor volume expands.

To determine the velocity, $\mathbf{v}$, we use a Darcy-type law:

$$\mathbf{v} = -\nabla \phi \tag{15}$$

where ϕ is a potential.

From equation (14) and (15), we get an expression for the velocity, $\mathbf{v}$, that enables us to solve equations (7)-(10), (12).

Further details can be found in (Ribba et al., 2006a,b, 2009).

3.7. Endostatin-based treatment

We considered a single intratumoral administration of adenoviruses encoding the endostatin gene. We supposed that this treatment would induce an increase in endostatin production by proliferative and quiescent tumor cells. We therefore modeled this administration by adding a

production term to the equation (4):

$$0 = \nabla \cdot (D_{endos} \, \nabla[endos]) + \alpha_{endos} \, (P + Q) - \beta_{endos} \, n - \delta_{endos} \, [endos]$$

$$+ \underbrace{C_{endos} \, \alpha_{endos} \, (P + Q) \, \mathbb{1}_{[t_1;t_2]}}_{overproduction \ due \ to \ treatment} \quad (16)$$

where C_{endos} denotes the overproduction rate, and $[t_1; t_2]$ represents the time interval over which endostatin is overproduced.

The overproduction rate can be linked to the dose or strength of the treatment, whereas the overproduction time interval can be linked to duration of treatment.

3.8. Summary of the model

Table 2 shows a summary of the macroscopic mathematical model, and Table 3 a summary of the molecular model. A summary of the parameters used for the computations is presented in Table 4 of the Appendix B.

3.9. Evaluation of therapeutic effects

As intratumoral administrations of adenoviruses encoding the endostatin gene are intended to slow tumor growth by delaying the development of a vascular network, we have introduced two criteria for the comparison of the benefits of treatment, illustrated in Figure 5.

Simulating the treatment administration at the very early stage of tumor growth, we first considered the time taken for the tumor to grow to more than a given size represented by the threshold τ_g. In this criterion, the duration of treatment (interval $[t_1; t_2]$ in equation (16)) was integrated into the time considered. Consequently, we also considered the time between the end of treatment (i.e. t_2) and the time when the tumor size exceeded the threshold τ_g.

Obviously, the greater these criteria, the more effective the treatment.

22

Entity	Model equation
Density of unstable endothelial cells (ECs)	$\partial_t n = \nabla \cdot (D_e\, \nabla n) + \alpha\, n\, \left(1 - \frac{n+n_S}{N_{max}}\right) - \nabla \cdot \left(\chi\, n\, \left(1 - \frac{n+n_S}{N_{max}}\right) \nabla[VEGF]\right) - \partial_t n_S$
Density of stable ECs	$\partial_t n_S = \mu\, H(E_{Ang1} - E_{Ang1_{min}})\, H(n + n_S - N_{min})\, n$
Concentration of VEGF	$0 = \nabla \cdot (D_V\, \nabla[VEGF]) + \alpha_V\, Q - \beta_V\, n - \delta_V\, [VEGF]$
Concentration of endostatin	$0 = \nabla \cdot (D_{endos}\, \nabla[endos]) + \alpha_{endos}\,(P + Q) - \beta_{endos}\, n - \delta_{endos}\, [endos]$ $\qquad\qquad\qquad\qquad\qquad + C_{endos}\, \alpha_{endos}\,(P + Q)\, \mathbb{1}_{[t_1;t_2]}$
Concentration of angiopoietin-1	$[Ang1] = [Ang1]_0$
Concentration of angiopoietin-2	$0 = \nabla \cdot (D_{A2}\, \nabla[Ang2]) + \alpha_{1,A2}\,(P + Q) + \alpha_{2,A2}\, n - \beta_{A2}\, n - \delta_{A2}\, [Ang2]$
Concentration of oxygen	$0 = \nabla \cdot (D_O\, \nabla[O_2]) - (\beta_{1,O}\, P + \beta_{2,O}\, Q + \beta_{3,O}\, M)\, [O_2] - \delta_O\, [O_2]$ $[O_2] = [O_2]_{max}$ where $n_S \neq 0$
Density of proliferative tumor cells	$\partial_t P_1 + \partial_a P_1 + \nabla \cdot (\mathbf{v}\, P_1) = 0 \qquad\qquad \partial_t P_2 + \partial_a P_2 + \nabla \cdot (\mathbf{v}\, P_2) = 0$ $P_1(a=0) = 2P_2(a = a_{max,P_2}) \qquad P_2(a=0) = fP_1(a = a_{max,P_1}) + [\partial_t f]^+ Q(t^-)$
Density of quiescent tumor cells	$\partial_t Q + \nabla \cdot (\mathbf{v}\, Q) = g\,(1 - f)\, P_1(a = a_{max,P_1}) - [\partial_t f]^+ Q(t^-) + [\partial_t g]^- Q(t^-)$
Density of apoptotic tumor cells	$\partial_t A + \nabla \cdot (\mathbf{v}\, A) = (1 - g)\, P_1(a = a_{max,P_1}) - [\partial_t g]^- Q(t^-)$
Density of healthy cells	$\partial_t M + \nabla \cdot (\mathbf{v}\, M) = 0$

Table 2: Summary of the equations of the macroscopic model.

3.10. Boundary and initial conditions

Boundary conditions. We assumed that the various quantities in our mathematical model did not cross the boundary of the computational domain (Ω). This can be modeled by setting Neumann conditions at the boundary of the model:

$$\frac{\partial n}{\partial \vec{\nu}}\Big|_{\partial \Omega} = 0, \quad \frac{\partial n_S}{\partial \vec{\nu}}\Big|_{\partial \Omega} = 0, \quad \frac{\partial [VEGF]}{\partial \vec{\nu}}\Big|_{\partial \Omega} = 0, \quad \frac{\partial [endos]}{\partial \vec{\nu}}\Big|_{\partial \Omega} = 0, \quad \frac{\partial [Ang2]}{\partial \vec{\nu}}\Big|_{\partial \Omega} = 0, \quad \frac{\partial [O_2]}{\partial \vec{\nu}}\Big|_{\partial \Omega} = 0$$

where $\vec{\nu}$ represents the outgoing normal vector to Ω boundary and $\frac{\partial}{\partial \vec{\nu}}$ is defined by:

$$\frac{\partial \zeta}{\partial \vec{\nu}} = \nabla \zeta \cdot \vec{\nu} \qquad \text{for all function } \zeta \text{ defined on } \Omega.$$

23

Parameter	Description	Expression	Equation
D_e	Rate of diffusion of endothelial cells (ECs)	$C_e * \lambda_{e,d}$	(1)
α	Rate of proliferation of ECs	$PA(E_{VEGF,prolif}) * \lambda_{e,p} \quad$ where $$E_{VEGF,prolif} = \frac{Emax_{VEGF,prolif}}{1+\frac{K_{D,VEGF}}{[VEGF]}\left(1+\frac{[endos]}{K_{D,endos}}\right)}$$	(1)
χ	Rate of chemotaxis of ECs	$\lambda_{e,c} \dfrac{Emax_{VEGF,chemo}}{1+\frac{K_{D,VEGF}}{[VEGF]}\left(1+\frac{[endos]}{K_{D,endos}}\right)}$	(1)
E_{Ang1}	Effect of angiopoietin-1 on maturation	$\dfrac{Emax_{Ang1}}{1+\frac{K_{D,Ang1}}{[Ang1]}\left(1+\frac{[Ang2]}{K_{D,Ang2}}\right)}$	(2)
β_V	Binding rate of VEGF to Flk-1	$\dfrac{\beta_{max,V}}{1+\frac{K_{D,VEGF}}{[VEGF]}\left(1+\frac{[endos]}{K_{D,endos}}\right)}$	(3)
β_{endos}	Binding rate of endostatin to Flk-1	$\dfrac{\beta_{max,endos}}{1+\frac{K_{D,endos}}{[endos]}\left(1+\frac{[VEGF]}{K_{D,VEGF}}\right)}$	(4)
β_{A2}	Binding rate of angiopoietin-2 to Tie2	$\dfrac{\beta_{max,A2}}{1+\frac{K_{D,A2}}{[Ang2]}\left(1+\frac{[Ang1]}{K_{D,A1}}\right)}$	(5)

Table 3: Summary of the molecular model.

Initial conditions. We simulated the mathematical model presented here in two dimensions. The computational domain was a square.

In our simulation settings, the tumor is circular and stands in the middle of the domain. We considered the tumor to be surrounded by four pre-existing blood vessels composed of both stable and unstable endothelial cells (Figure 6).

At time zero of simulation, tumor density in the central cluster is given by a Gaussian distribution (see color degradation in the central tumor cluster in Figure 6). We also supposed that this tumor was composed of both proliferative and quiescent cells with:

$$P_1(\mathbf{x}, t=0, a) = P_2(\mathbf{x}, t=0, a) \leq Q(\mathbf{x}, t=0) \quad \forall \mathbf{x} \in \Omega, \ \forall a \tag{17}$$

Initially, the endothelial cells are uniformly distributed in the clusters representing existing blood vessels, with:

$$n_S(\mathbf{x}, t=0) = 2n(\mathbf{x}, t=0) = \frac{N_{max}}{2} \quad \forall \mathbf{x} \in \Omega \tag{18}$$

The initial concentrations of VEGF, endostatin, angiopoietin-2 and oxygen are set to be equal to the steady-state solution of their respective equations (equations (3)-(6)).
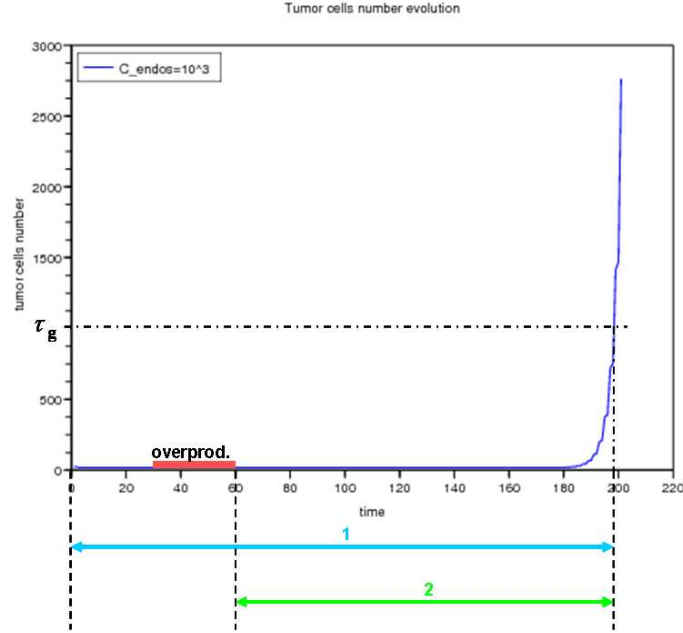
24

Figure 5: The two criteria used to evaluate treatment efficacy. Criterion 1 represents the time required by the tumor to exceed a given size threshold (denoted by τ_g). This time includes the treatment period. Criterion 2 is the time interval between the end of treatment and growth of the tumor above the threshold τ_g.

4. Numerical results

We simulated the computational model, with the initial conditions mentioned above, on a 100*100 discrete elements grid. The partial differential equations of our model were discretized using a finite volume method. We also used a penalization method to ensure that the concentration of oxygen was fixed in the functional blood vessels. Our time unit is the half-day (12 hours (h)), and our space unit is the millimeter (mm).

4.1. Tumor growth and angiogenesis without treatment

We first present simulation results of the model in the absence of treatment (see Figure 7).

Initially, the tumor cells consume the oxygen available in their environment as a result of diffusion from the existing oxygen sources. As the tumor cells proliferate, the local oxygen concentration
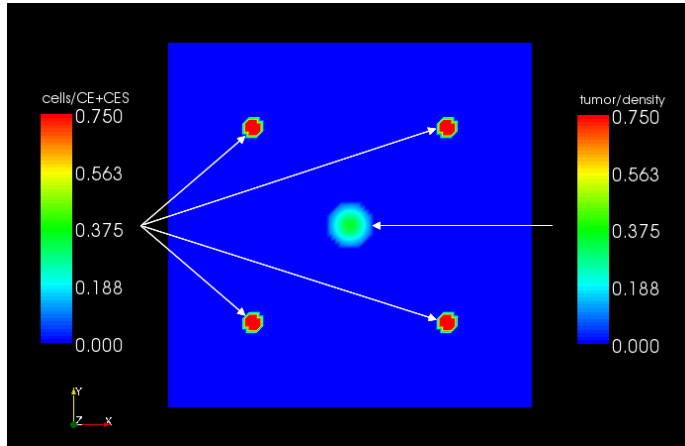
25

Figure 6: Initial conditions of the densities of unstable and stable endothelial cells and of tumor cells. Tumor cells are located in the middle of the domain. Four existing blood vessels composed of endothelial cells surround the tumor.

soon becomes inadequate, and hypoxia occurs. Proliferative tumor cells revert to the quiescent state, and those subjected to the most severe hypoxia (primarily in the center of the tumor) simply die (they move into the apoptotic compartment and no longer appear in any of the pictures). In response to hypoxic stress, quiescent cells secrete VEGF. VEGF molecules diffuse into the domain, reach the endothelial cells, and stimulate the unstable cells to proliferate and migrate towards tumor cells (see Figure 7, $t = 10$). Through the process of maturation described above, endothelial cells form functional blood vessels (see Figure 7, $t = 30$ and $t = 70$).

As soon as the local concentration of oxygen increases in the tumor region as a result of the formation of new vessels, the peripheral tumor cells begin to proliferate (see Figure 7, $t = 145$).

At the end of this simulation, the tumor is composed of an apoptotic center, surrounded by quiescent cells, which in turn are surrounded by proliferative cells (see Figure 7, $t = 159$). This configuration is consistent, for instance, with conventional subcutaneous xenografted mouse models.

4.2. Endostatin-based treatment effects

The model was then used to simulate the effect of endostatin overproduction from $t = 30$ to $t = 60$, as described in section 3.7 ($C_{endos} = 100$). Figure 8 depicts the change in endothelial cell density during simulated treatment (left panel) compared to the untreated condition (right panel).
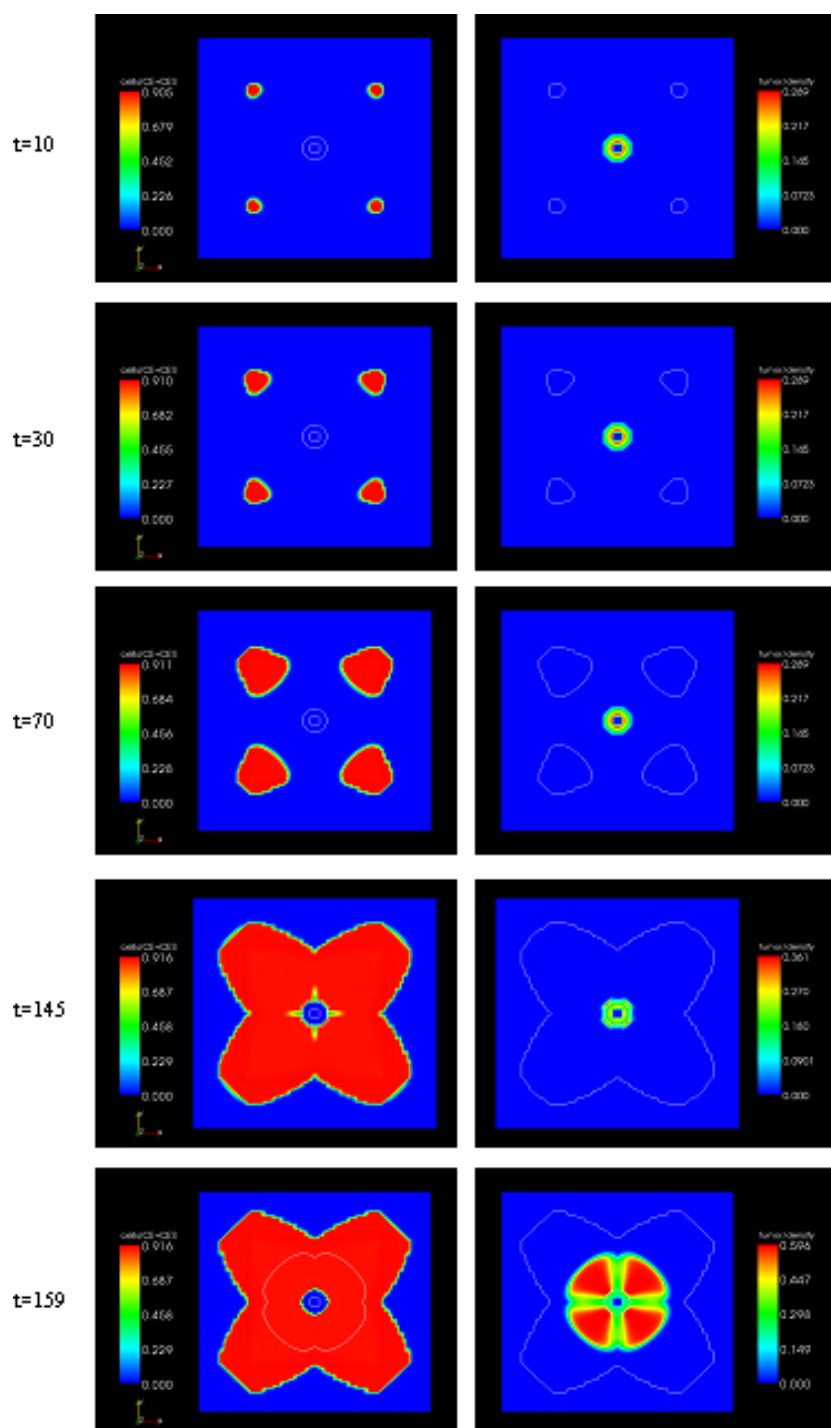
Figure 7: From top to bottom: spatio-temporal evolution of the densities of endothelial cells (unstable plus stable) and tumor cells. Left panel, pictures show the spatio-temporal evolution of endothelial cells (density) proliferating and migrating from the existing vessels towards the tumor cells. The fine contour line demarcates the area of the tumor. Right panel, pictures show the spatio-temporal evolution of tumor cell density. The fine contour line demarcates the distribution of endothelial cells.

In the early stages of simulation, there is no change in the behavior of the system (see Figure 8, $t = 25$). Subsequently, endostatin overproduction leads to regression of the vasculature (see Figure 8, $t = 45$). This results from the binding of endostatin molecules to Flk-1 receptors instead of VEGF molecules. As a consequence, the unstable endothelial cells are no longer sufficiently stimulated, and some of them die. However, as soon as endostatin overproduction stops, angiogenesis starts again (see Figure 8, $t = 65$). Nevertheless, the treatment has induced a delay in vessel growth, and at the end of the simulation phase, as expected, tumor vasculature is less developed in the treated condition, as a consequence of endostatin overproduction (see Figure 8, $t = 159$). This delay in blood vessel formation leads to slower tumor growth, as shown in Figure 9.

We further compared the change in tumor density in the presence and absence of endostatin overproduction by analyzing the change in the sum of proliferative and quiescent tumor cells and that in the sum of endothelial cells throughout the whole computation model. As shown in Figure 10, endostatin overproduction delays endothelial cell proliferation, and in consequence slows tumor growth.

4.3. Influence of treatment design

In what follows, we use the treatment efficacy criteria presented in section 3.9 to analyze the influence of treatment design on tumor growth. In our computation model, treatment or endostatin overproduction, is characterized by two factors: the duration of overproduction, and the degree of overproduction (coefficient C_{endos} in equation (16)). The former can be assimilated to treatment duration, and the second to the dose or strength of the treatment.

Figure 11 shows the time course of efficacy criterion 1 (the total time taken for the tumor to grow above a given threshold after treatment stops) with respect to the degree of overproduction (or overproduction rate) and for different overproduction durations. It soon becomes apparent that it might be more effective to increase the duration of overproduction rather than increasing its degree.

All the curves depicted display three phases: a gradual increase, followed by a transient sharp increase and finally a plateau. At low overproduction rates, the time course of the efficacy criterion evolution is the outcome of a classical model of competition between agonists and antagonists at a given receptor. In our model, endostatin competes with VEGF, which activates the proliferation
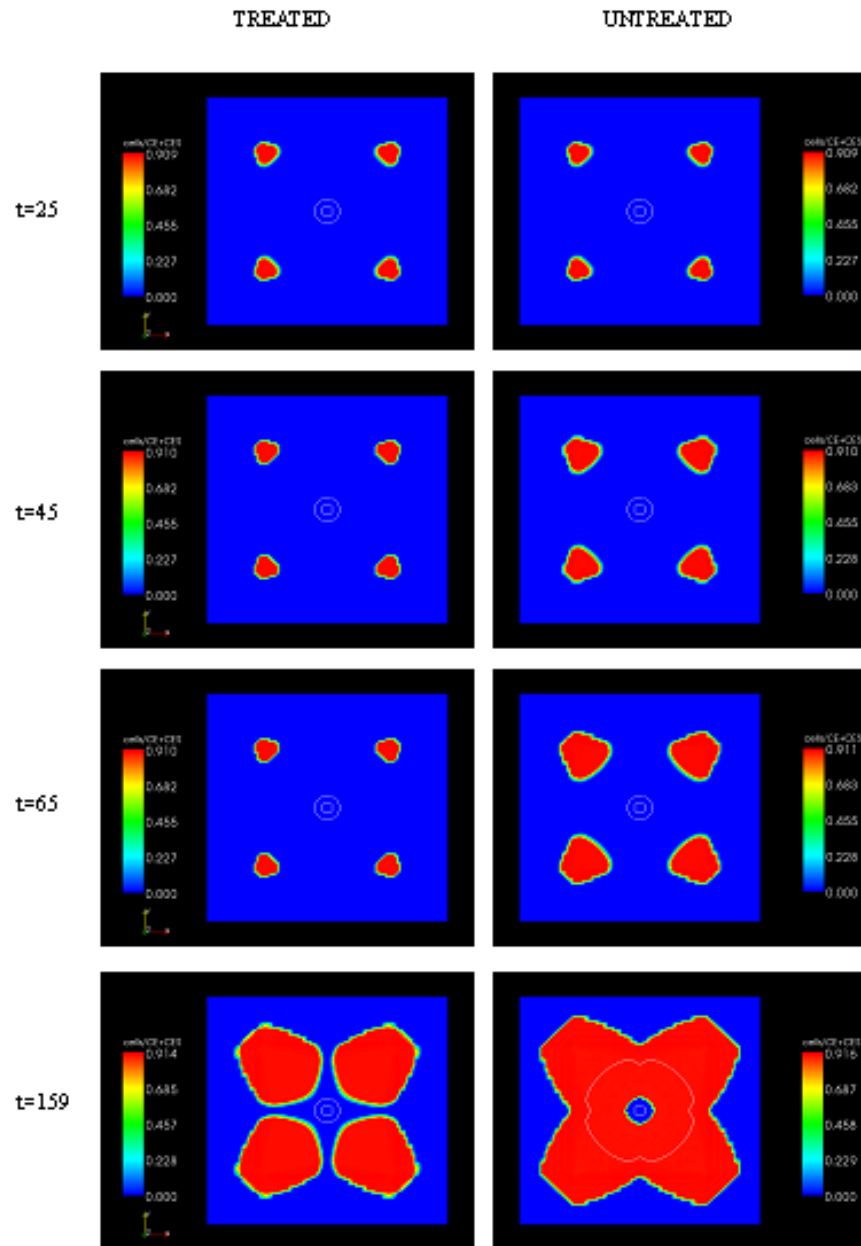
28

Figure 8: From top to bottom: spatio-temporal evolution of endothelial cell density with (left panel) and without (right panel) endostatin overproduction (from $t = 30$ to $t = 60$). The fine contour line outlines the tumor.
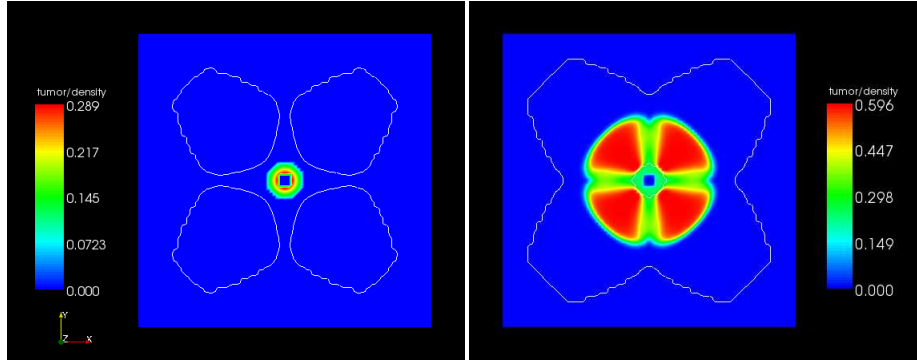
Figure 9: Tumor density at time $t = 159$ (end of simulation) with (left panel) and without (right panel) endostatin overproduction. The fine contour line outlines the endothelial cells.
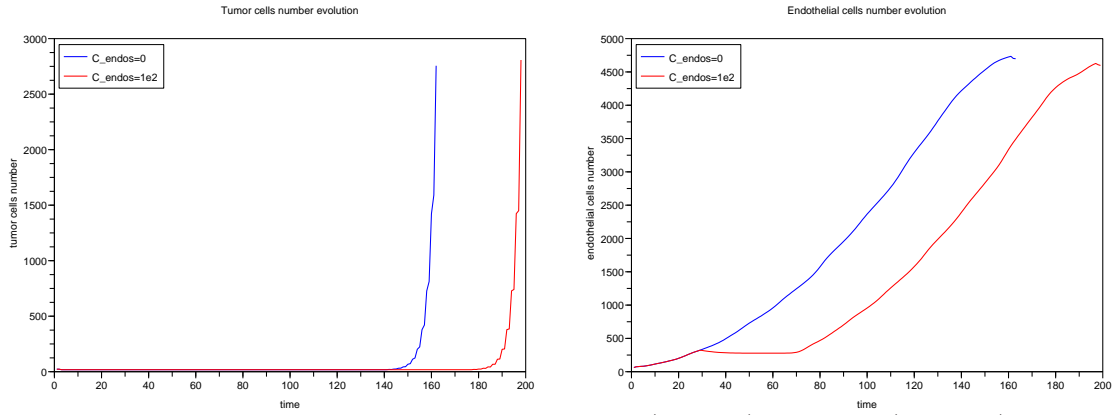

Figure 10: Left: time course of the total number of tumor cells with (red curve) and without (blue curve) treatment. Right: the same for the total number of endothelial cells (unstable plus stable).

and migration of endothelial cells, to bind to the Flk-1 receptor (see section 3.1). A switch occurs when the concentration of endostatin becomes too high relative to that of VEGF. Consequently, the unstable endothelial cells proliferate less, and tend to die (see Figure 3), leading to a sharp increase in the efficacy criterion. Finally, the system tends towards a classical saturation phase, during which the endostatin concentration is such that VEGF cannot bind to Flk-1 receptors anymore. The proliferation rate of the endothelial cells reaches its lowest (negative) value (see Figure 3).

Interestingly, analyzing the same behavior for criterion 2 (time between stopping treatment and the tumor's reaching a size above a given threshold) leads to a different overall curve pattern (see Figure 12).
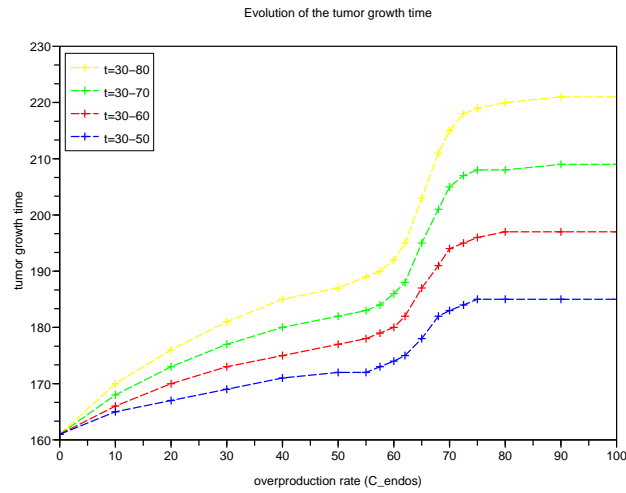
30

Figure 11: Change in the tumor growth time criterion depending on variations in the degree and duration of the overproduction (one curve for each duration).
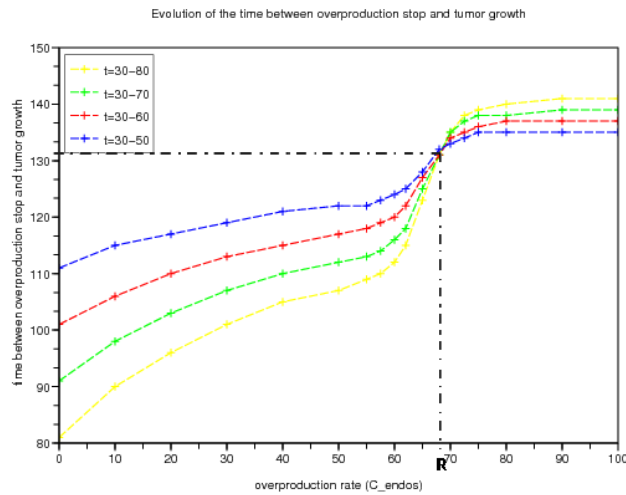
Figure 12: Change in the time between the cessation of overproduction and reaching a tumor size above the critical threshold, depending on variations in the rate and duration of the overproduction. All the curves intersect at one point corresponding to an overproduction rate denoted by "R".

As can be seen in Figure 12, the curves intersect at a single point. This means that there is an overproduction rate (referred to as "R" in what follows) for which efficacy criterion 2 remains unchanged despite an increase in the duration of treatment. "R" corresponds to the endostatin

31

overproduction rate that leads to an unstable endothelial cell proliferation rate equal to 0. If this happens, angiogenesis is not simply reduced, but stops completely; consequently, however long the treatment lasts, angiogenesis starts again under the same conditions as pertained when it stopped. Analyzing the system using criterion 2, which "eliminates" the duration of treatment, naturally leads to a steady state situation at this point. For overproduction rates of less than "R", lengthening the duration of treatment has a deleterious effect, as the tumor starts growing more quickly after treatment stops. This is known as the "rebound" effect. In our model, this results from inhibition of VEGF binding to Flk-1 receptors, thus increasing the concentration of free VEGF (since, although angiogenesis is slowed, the quiescent tumor cells still produce VEGF). As soon as the treatment stops, VEGF massively binds to Flk-1 receptors, leading to rapid endothelial cell proliferation and powerful activation of the angiogenic process. In contrast, for endostatin overproduction rates above "R", simulations indicate that there is a slight therapeutic advantage as result of lengthening the duration of treatment. This results from the decrease in the number of unstable endothelial cells as a result of a high concentration of endostatin (see Figure 3), leading to a decrease in the number of Flk-1 receptors. In consequence, the rebound effect is damped down.

This simple analysis highlights the difficulty of optimizing treatment design, as efficacy may depend on the multiscale features of the processes of tumor growth and angiogenesis.

5. Discussion

The process of tumor angiogenesis is recognized as being a key process in tumor development. In consequence, anti-angiogenesis therapies are being investigated throughout the world as a promising way to treat cancer patients. In this paper, we propose a mathematical model of angiogenesis and tumor growth. This model is based on a set of partial differential equations that describe the behavior of endothelial cells, that constitute blood vessel walls, tumor cells, as well as of some major pro- and anti-angiogenic substances, such as vascular endothelial growth factor (VEGF), endostatin, angiopoietin-1 and angiopoietin-2. At the molecular level, the model focuses on VEGF/endostatin competition to bind to Flk-1 receptors, and on angiopoietin-1/angiopoietin-2 competition to bind

32

to Tie2 receptors. These binding processes regulate the whole process of blood vessel formation. At the macroscopic level, the model describes the spatio-temporal patterns of stable and unstable endothelial cells and tumor cells during the different phases of the cell cycle.

Compared to most of the existing models, this new model of angiogenesis offers an extra degree of complexity, particularly at the molecular level. This makes it possible to study the activation of angiogenesis related to the molecular properties of the main pro- and anti-angiogenic endogenous substances. As a result, this model could be used to analyze the impact of the molecular mechanisms of angiogenesis on the dynamics of tumor growth.

By injecting adenoviruses directly into the tumor mass, endostatin gene therapy triggers an increase in the production of endostatin by tumor cells, thus resulting in higher local expression of this VEGF antagonist. By simulating the effect of endostatin gene therapy on the system, we highlighted the existence of a critical treatment dose (referred to as a critical rate of endostatin overproduction). Below this threshold dose, increasing the duration of the treatment can actually have a deleterious effect due to the emergence of a rebound effect in the angiogenesis process. In contrast, above this critical dose, increasing the duration of treatment may improve its efficacy. Interestingly, these results show some similarity to those reported by Ribba and colleagues in (Ribba et al., 2006b), where the authors used a multiscale, avascular tumor growth model to investigate the effects of anti-invasive treatments.

At this point, we should point out the main limitations of our work. First of all, the study presented here is a qualitative study. The model used is so complex, in particular due to its spatial structure, that it cannot be used as a quantitative tool. Nevertheless, a qualitative analysis of this type can still be used in a multiscale manner to investigate complex questions, such as how to optimize innovative anti-cancer drug delivery. However, some of the parameters, in particular those used in the pharmacological laws, can be estimated or quantified on the basis of existing published results.

One of the major discussion issues relates to our decision to model the angiogenesis process by means of continuous partial differential equations. Several previous publications have presented continuous angiogenesis models, but discrete models seemed to be more relevant for modeling the formation of blood vessels. However, as in any modeling experiment, the choice of mathematics

33

should depend on the objective of the study. In our case, we claim that a continuous model is sufficient to qualitatively analyze how efficient molecular-targeting angiogenesis drugs are. Obviously, in some cases, this may not be the case. For instance, some anti-VEGF drugs, such as Bevacizumab (Avastin, Roche), are known to modify vessel structure and are also thought to homogenize tumor vasculature. In this particular case, discrete models would be required, in particular to integrate important factors such as the permeability of blood vessels. However, most innovative cytostatic drugs impact on the molecular mechanisms of angiogenesis rather than directly affecting the structure of newly-formed blood vessels.

Some of the modeling hypotheses we used are also open to question. From a biological point of view, we are aware that we chose to ignore some phenomena that could be seen as key processes in vascular tumor growth but, for this first study, we had to compromise between the consistency of the model and its complexity. For this first step in our investigations, we chose to focus on the main mechanisms involved in vascular tumor growth in order to be able to analyze the global impact of anti-angiogenic substances. Nevertheless, we implemented the model in a way that would make it easier in the future to include additional biological phenomena.

In future work, we plan to consider several extensions of the model proposed in this paper. For instance, we have not so far taken various biomechanical aspects into account. These aspects can affect the growth both of the tumor and of the vascular network. We currently assume that the motion of the tumor cells is solely due to cell division. In fact, some biomechanical phenomena, such as the mechanical stress exerted by the surrounding host tissue, and cell-cell and cell-extracellular matrix adhesion, are also known to impact on tumor growth (see (Kumar and Weaver, 2009) for a review). We could take these biomechanical effects on tumor growth into account on the basis of the work of Bresch and colleagues (Bresch et al., 2009a,b), Gerisch and Chaplain (Gerisch and Chaplain, 2008), or Araujo and McElwain (Araujo and McElwain, 2005a,b). Stress, cell-cell and cell-extracellular matrix adhesion can also affect endothelial cells, and, in our work, we took the natural affinity of endothelial cells for one another into account (see Section 3 for details). We could also consider haptotaxis as Anderson and Chaplain did (Anderson and Chaplain, 1998), haptotaxis being the sensitivity of endothelial cells to the concentration gradient of some endogenous substances promoting adhesion to the extracellular matrix. We could also draw inspiration from the work of Tosin and colleagues (Tosin et al., 2006), where the authors introduced an internal force within the

34

population of endothelial cells, and modeled the interactions between the endothelial cells and the extracellular matrix involving an elastic force.

We could also take biomechanical interactions between the tumor and the vascular network into account. For instance, a phenomenon of vascular collapse and regression in tumors has been experimentally observed (Goldacre and Sylven, 1962). This phenomenon is still poorly understood, but could be a consequence of the interstitial pressure, or of biomechanical stresses more generally, created by the growing tumor mass (Boucher et al., 1990). Vascular collapse and regression is responsible for reducing the supply of nutrients and oxygen and so, potentially, for inducing quiescence in tumor cells. Starting from the model we propose in this paper, we could assume that the behavior of the density of mature endothelial cells depends on the pressure created by the growing tumor mass. If this pressure becomes too high, mature endothelial cells might return to the immature state and die. Araujo and colleagues have developed some mathematical models of the genesis of stress in growing tumors to analyze the nature and the distribution of the biomechanical stresses induced by the growth of the tumor mass (Araujo and McElwain, 2005b,c). Moreover, the role of such biomechanical stresses in vessel collapse and regression, and so in the supply of nutrients and oxygen, has already been studied using various mathematical models (Baxter and Jain, 1989; Araujo and McElwain, 2004, 2006; Macklin et al., 2009), which we could draw on to extend our present model. This could be a good way to model vessel regression, and thus to analyze the effect of such biomechanical stresses on the development of the vascular network and so on the efficacy of anti-angiogenic treatment.

Moreover, on the basis of the equations we propose in this paper, a three-dimensional model could be more realistic. It would also be interesting to test other kinds of 2D geometries, as these might produce different results.

Finally, with regard to modeling the action of the treatment, it could be interesting to develop a more mechanistic approach by taking adenovirus diffusion inside the tumor mass into account, as well as the immune response, and to investigate the influence of such treatment-related parameters on the overall efficacy on tumor growth and angiogenesis.

Nevertheless, we believe that this modeling approach can be considered for use as a first qualitative investigation of the effect of a treatment strategy. If our results are confirmed, it will be important for clinicians to identify the critical dose in order to optimize endostatin-based treatment

delivery.

More generally, our present study highlights the difficulty of determining the appropriate anti-angiogenic treatment strategy. We note that, depending on the treatment schedule, anti-angiogenic treatment can actually be responsible for increasing the local invasiveness of the tumor. This is one of the adverse consequences of anti-angiogenic therapies recently described in (Bergers and Hanahan, 2008; Ebos et al., 2009; Pàez-Ribes et al., 2009). In (Bergers and Hanahan, 2008), the authors proposed some explanations of the fact that anti-VEGF therapies can have both favorable and deleterious effects on patients' health as a result of increasing the growth of both the primary tumor and its metastases. Collecting data from the literature, they hypothesized two modes of resistance to anti-VEGF treatment: evasive resistance, i.e. an adaptation of the tumor to the presence of the angiogenesis inhibitor, and intrinsic resistance, i.e. a pre-existing lack of responsiveness of the tumor. Pàez-Ribes and colleagues have also demonstrated the evasive resistance to anti-VEGF in two mouse models of cancer (Pàez-Ribes et al., 2009). Ebos and colleagues have shown that, depending on the duration and dose of the treatment, the inhibition of the VEGF receptor by the same drug can lead to opposite effects on tumor growth (Ebos et al., 2009). They illustrated the fact that microenvironmental changes in organs, possibly due, for instance, to previous cancer treatments, could induce intrinsic resistance in the tumor to an angiogenesis inhibitor.

These studies tend to suggest that anti-angiogenic molecules should be combined with cytotoxic therapy, for instance with chemotherapy, as is usually indicated for Bevacizumab, in order to improve their efficacy against cancer development, i.e. against the development of both the primary tumor and its metastases, or at least to reduce the occurrence of some deleterious events. The model we propose in this paper could provide a way of optimizing cancer treatment by investigating the optimum combination of anti-angiogenic molecules with chemotherapy.

6. Acknowledgements

A. The *Emax* model

A.1. Effect of an agonist

A ligand can activate or inhibit the receptor to which it binds. If binding results in activation, the ligand is called an agonist, and if it results in inhibition, it is called an antagonist. The binding of an agonist to a receptor induces a specific effect. This effect depends on the ligand's binding capacities, also known as the affinity of the ligand for the receptor. This affinity is measured in terms of the dissociation constant (usually denoted by K_D), which is the concentration of agonist bound to 50% of the receptors of a cell membrane.

The relation between the concentration of agonist (dose) and the effect induced is given by the following expression, also known as the *Emax* model:

$$E = \varepsilon \frac{E_{max}}{1 + \frac{K_D}{[C]}}$$

where:

- E denotes the effect of the agonist;

- $\varepsilon \leq 1$ models the agonist intrinsic activity, i.e. its ability to activate the receptor; if $\varepsilon = 1$, the intrinsic activity is maximal and the agonist is said to be a complete agonist; if $\varepsilon < 1$, the agonist is said to be a partial agonist;

- E_{max} is the maximum effect the agonist can induce by binding to the receptor;

- K_D is the dissociation constant of the agonist at the receptor;
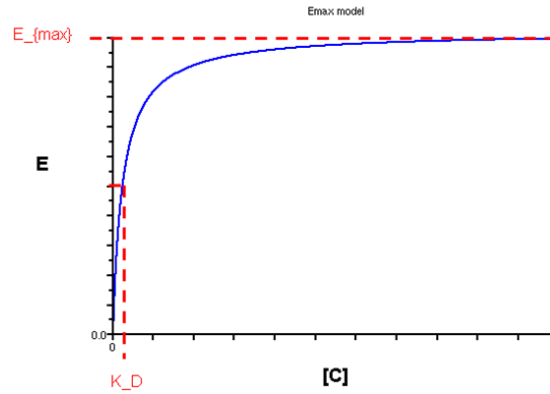
- $[C]$ denotes the agonist concentration.

Figure 13: Change of the effect (E) with agonist concentration ($[C]$). E_{max} denotes the maximum effect; K_D is the dissociation constant of the agonist at the receptor.

For instance, in the case of tumor-induced angiogenesis, VEGF acts as an agonist at the Flk-1 receptor, and angiopoietin-1 is an agonist at the Tie2 receptor. We assumed that both VEGF and angiopoietin-1 are complete agonists ($\varepsilon = 1$).

A.2. Effect of an agonist in the presence of a competitive antagonist

A competitive antagonist is a substance that can bind to the receptor at the same binding site as the agonist. When it does so, this prevents the agonist from binding to this receptor, and thus decreases the effect produced by the agonist by reducing its affinity for the receptor (that is by shifting the dose-effect relationship (described in A.1) to the right). So, the effect (E) of an agonist in the presence of a competitive antagonist is given by:

$$E = \varepsilon \frac{E_{max}}{1 + \dfrac{K_D}{[C]}\left(1 + \dfrac{[A]}{K_{D,A}}\right)}$$

where:

38

- ε, E_{max}, K_D, $[C]$ are described in A.1;

- $[A]$ denotes the concentration of the antagonist;

- $K_{D,A}$ is the dissociation constant of the antagonist at the receptor.

For instance, in the case of angiogenesis, endostatin is a competitive antagonist of VEGF at the Flk-1 receptor, and angiopoietin-2 is a competitive antagonist of angiopoietin-1 at the Tie2 receptor.

Unlike competitive antagonists, some substances can decrease the effect of the agonist by binding to a different binding site: they are known as noncompetitive antagonists. The antagonists we consider in our model are all competitive antagonists, and so we will not describe the effect of an agonist in the presence of an uncompetitive antagonist.

B. Summary of the model parameters

In this section, we use the following notations: h (hour), mm (millimeter), M (molarity).

Table 4 shows a summary of the parameters used for the computations.

Parameter	Description	Value	Units	Equation	Reference
D_e	Rate of diffusion of endothelial cells (ECs)	$6.25\text{e-}8 * \begin{cases} 0.5 & if\ P+Q > 0.12 \\ 1 & else \end{cases}$	$\text{mm}^2.\text{h}^{-1}$	(1)	
N_{max}	Maximum density of ECs	1	cells.mm^{-2}	(1)	
$Emax_{VEGF,prolif}$	Maximum effect of VEGF on EC proliferation	$5*10^{-2}$	h^{-1}	(1)	
Ap	Maximum death rate of ECs	$-2*10^{-2}$	h^{-1}	(1)	
$Emin_{prolif}$	Minimum value of $E_{VEGF,prolif}$ below which the EC proliferation rate becomes negative	$2*10^{-2}$	h^{-1}	(1)	
$\lambda_{e,p}$	Restriction function of EC proliferation	$\begin{cases} 0.5 & if\ P+Q > 0.12 \\ 1 & else \end{cases}$	-	(1)	
$Emax_{VEGF,chemo}$	Maximum effect of VEGF on EC chemotaxis	$1.25*10^{-2}$	$\text{mm}^2.\text{M}^{-1}.\text{h}^{-1}$	(1)	
$\lambda_{e,c}$	Restriction function of EC chemotaxis	$\begin{cases} 0.5 & if\ P+Q > 0.12 \\ 1 & else \end{cases}$	-	(1)	
$Emax_{Ang1}$	Maximum effect of angiopoietin-1 on ECs	$2*10^{-1}$	h^{-1}	(2)	
$E_{Ang1_{min}}$	Minimum value of E_{Ang1} required for maturation	$5*10^{-1}$	h^{-1}	(2)	
N_{min}	Minimum value of EC density required for maturation	$9*10^{-1}$	cells.mm^{-2}	(2)	
μ	Maturation rate of ECs	1	h^{-1}	(2)	
D_V	Diffusion rate of VEGF	$1.875*10^{-1}$	$\text{mm}^2.\text{h}^{-1}$	(3)	(Gabhann and Popel, 2005)(Addison-Smith et al., 2008)

Table 4: Summary of the model parameters.

Parameter	Description	Value	Unity	Equation	Reference
α_V	Production rate of VEGF	2.11	M.cells^{-1}.mm^2.h^{-1}	(3)	
$\beta_{max,V}$	Maximum binding rate of VEGF to Flk-1	$1.25*10^{-3}$	M.cells^{-1}.mm^2.h^{-1}	(3)	
$K_{D,VEGF}$	Dissociation constant of VEGF at Flk-1	10^{-7}	M	(1)(3)(4)	
δ_V	Degradation rate of VEGF	$1.25*10^{-4}$	h^{-1}	(3)	
D_{endos}	Diffusion rate of endostatin	$2.38*10^{-1}$	mm^2.h^{-1}	(4)	
α_{endos}	Production rate of endostatin	10	M.cells^{-1}.mm^2.h^{-1}	(4)	
$\beta_{max,endos}$	Maximum binding rate of endostatin to Flk-1	$1.25*10^{-3}$	M.cells^{-1}.mm^2.h^{-1}	(4)	
$K_{D,endos}$	Dissociation constant of endostatin at Flk-1	$2*10^{-4}$	M	(1)(3)(4)	
δ_{endos}	Degradation rate of endostatin	$1.25*10^{-4}$	h^{-1}	(4)	
C_{endos}	Rate of endostatin overproduction due to treatment	variable	M.cells^{-1}.mm^2.h^{-1}	(16)	
$[Ang1]_0$	Concentration of angiopoietin-1	$4*10^{-2}$	M	-	
$K_{D,Ang1}$	Dissociation constant of angiopoietin-1 at Tie2	$3*10^{-9}$	M	(2)	(Maisonpierre et al., 1997)
D_{A2}	Diffusion rate of angiopoietin-2	$4.5*10^{-3}$	mm^2.h^{-1}	(5)	
$\alpha_{1,A2}$	Rate of angiopoietin-2 production by tumor cells	$3*10^{-4}$	M.cells^{-1}.mm^2.h^{-1}	(5)	
$\alpha_{2,A2}$	Rate of angiopoietin-2 production by ECs	$1.5*10^{-4}$	M.cells^{-1}.mm^2.h^{-1}	(5)	

Table 4: Summary of the model parameters (Contd).

$\beta_{max,A2}$	Maximum binding rate of angiopoietin-2 to Tie2	$3*10^{-6}$	$M.cells^{-1}.mm^2.h^{-1}$	(5)	
$K_{D,Ang2}$	Dissociation constant of angiopoietin-2 at Tie2	$3*10^{-9}$	M	(2)(5)	(Maisonpierre et al., 1997)
δ_{A2}	Degradation rate of angiopoietin-2	$1.25*10^{-5}$	h^{-1}	(5)	
D_O	Diffusion rate of oxygen	1	$mm^2.h^{-1}$	(6)	(Takahashi et al., 1966)
$\beta_{1,O}$	Rate of oxygen consumption by proliferative tumor cells	3	$cells^{-1}.mm^2.h^{-1}$	(6)	
$\beta_{2,O}$	Rate of oxygen consumption by quiescent tumor cells	1.5	$cells^{-1}.mm^2.h^{-1}$	(6)	
$\beta_{3,O}$	Rate of oxygen consumption by healthy cells	$3.75*10^{-1}$	$cells^{-1}.mm^2.h^{-1}$	(6)	
$[O_2]_{max}$	Oxygen concentration in functional blood vessels	8	M	(6)	
δ_O	Degradation rate of oxygen	10^{-3}	h^{-1}	(6)	
a_{max,P_1}	Maximum duration of phase P_1	12	h	(9)-(11)	
a_{max,P_2}	Maximum duration of phase P_2	12	h	(11)(14)	
τ_0	Threshold of overpopulation	0.8	$cells.mm^{-2}$	(9)(11)	
$\tau_{1,h}$	Threshold of hypoxia	5.5	M	(9)(11)	
$\tau_{2,h}$	Threshold of severe hypoxia	1.52	M	(9)(10)	
N_0	Total density of tumor cells	1	$cells.mm^{-2}$	(13)(14)	
τ_g	Threshold number of tumor cells for efficacy criteria definitions	1000	cells	-	

Table 4: Summary of the model parameters (Contd).

References

Addison-Smith, B., McElwain, D. L. S., Maini, P. K., Jan 2008. A simple mechanistic model of sprout spacing in tumour-associated angiogenesis. J Theor Biol 250 (1), 1–15.

Ahmad, S. A., Liu, W., Jung, Y. D., Fan, F., Reinmuth, N., Bucana, C. D., Ellis, L. M., Sep 2001. Differential expression of angiopoietin-1 and angiopoietin-2 in colon carcinoma. a possible mechanism for the initiation of angiogenesis. Cancer 92 (5), 1138–1143.

Alarcón, T., Byrne, H., Maini, P., 2005. A multiple scale model for tumor growth. Multiscale Model Simul 3, 440–475.

Anderson, A. R. A., Chaplain, M. A. J., Sep 1998. Continuous and discrete mathematical models of tumor-induced angiogenesis. Bull Math Biol 60 (5), 857–899.

Araujo, R. P., McElwain, D. L. S., Jun 2004. New insights into vascular collapse and growth dynamics in solid tumors. J Theor Biol 228 (3), 335–346.

Araujo, R. P., McElwain, D. L. S., 2005a. A mixture theory for the genesis of residual stresses in growing tissues I: a general formulation. SIAM J Appl Math 65, 1261–1284.

Araujo, R. P., McElwain, D. L. S., 2005b. A mixture theory for the genesis of residual stresses in growing tissues II: solutions to the biphasic equations for a multicell spheroid. SIAM J Appl Math 66 (2), 447–467.

Araujo, R. P., McElwain, D. L. S., 2005c. The nature of the stresses induced during tissue growth. Applied Mathematics Letters 18, 1081–1088.

Araujo, R. P., McElwain, D. L. S., Feb 2006. The role of mechanical host-tumour interactions in the collapse of tumour blood vessels and tumour growth dynamics. J Theor Biol 238 (4), 817–827.

Ausprunk, D. H., Folkman, J., Jul 1977. Migration and proliferation of endothelial cells in preformed and newly formed blood vessels during tumor angiogenesis. Microvasc Res 14 (1), 53–65.

Bartha, K., Rieger, H., Aug 2006. Vascular network remodeling via vessel cooption, regression and growth in tumors. J Theor Biol 241 (4), 903–918.

Baxter, L. T., Jain, R. K., Jan 1989. Transport of fluid and macromolecules in tumors. i. role of interstitial pressure and convection. Microvasc Res 37 (1), 77–104.

Benjamin, L. E., Keshet, E., Aug 1997. Conditional switching of vascular endothelial growth factor (vegf) expression in tumors: induction of endothelial cell shedding and regression of hemangioblastoma-like vessels by vegf withdrawal. Proc Natl Acad Sci U S A 94 (16), 8761–8766.

Bergers, G., Hanahan, D., Aug 2008. Modes of resistance to anti-angiogenic therapy. Nat Rev Cancer 8 (8), 592–603.

Blagosklonny, M. V., Pardee, A. B., 2002. The restriction point of the cell cycle. Cell Cycle 1 (2), 103–110.

Boucher, Y., Baxter, L. T., Jain, R. K., Aug 1990. Interstitial pressure gradients in tissue-isolated and subcutaneous tumors: implications for therapy. Cancer Res 50 (15), 4478–4484.

Bresch, D., Colin, T., Grenier, E., Ribba, B., Saut, O., 2009a. Computational modeling of solid tumor growth: the avascular stage. SIAM Journal on Scientific Computing (in revision).

Bresch, D., Colin, T., Grenier, E., Ribba, B., Saut, O., 2009b. A viscoelastic model for avascular tumor growth. Discrete and Continuous Dynamical Systems (submitted).

Byrne, H. M., Chaplain, M. A., Jul 1996. Growth of necrotic tumors in the presence and absence of inhibitors. Math Biosci 135 (15), 187–216.

Davis, S., Aldrich, T. H., Jones, P. F., Acheson, A., Compton, D. L., Jain, V., Ryan, T. E., Bruno, J., Radziejewski, C., Maisonpierre, P. C., Yancopoulos, G. D., Dec 1996. Isolation of angiopoietin-1, a ligand for the tie2 receptor, by secretion-trap expression cloning. Cell 87 (7), 1161–1169.

DeVita, V. T., Hellman, S., Rosenberg, S. A., 2005. Cancer - Principles and Practice of Oncology, 7th Edition. Lippincott Williams and Wilkins.

Ebos, J. M. L., Lee, C. R., Cruz-Munoz, W., Bjarnason, G. A., Christensen, J. G., Kerbel, R. S., Mar 2009. Accelerated metastasis after short-term treatment with a potent inhibitor of tumor angiogenesis. Cancer Cell 15 (3), 232–239.

Etoh, T., Inoue, H., Tanaka, S., Barnard, G. F., Kitano, S., Mori, M., Mar 2001. Angiopoietin-2 is related to tumor angiogenesis in gastric carcinoma: possible in vivo regulation via induction of proteases. Cancer Res 61 (5), 2145–2153.

Ferrara, N., Jul 1999a. Molecular and biological properties of vascular endothelial growth factor. J Mol Med 77 (7), 527–543.

Ferrara, N., Sep 1999b. Role of vascular endothelial growth factor in the regulation of angiogenesis. Kidney Int 56 (3), 794–814.

Ferrara, N., Oct 2002. Vegf and the quest for tumour angiogenesis factors. Nat Rev Cancer 2 (10), 795–803.

Folkman, J., Jan 1990. What is the evidence that tumors are angiogenesis dependent? J Natl Cancer Inst 82 (1), 4–6.

Folkman, J., Dec 2002. Role of angiogenesis in tumor growth and metastasis. Semin Oncol 29 (6 Suppl 16), 15–18.

Folkman, J., Mar 2006. Antiangiogenesis in cancer therapy–endostatin and its mechanisms of action. Exp Cell Res 312 (5), 594–607.

Gabhann, F. M., Popel, A. S., Jun 2005. Differential binding of vegf isoforms to vegf receptor 2 in the presence of neuropilin-1: a computational model. Am J Physiol Heart Circ Physiol 288 (6), H2851–H2860.

Gerisch, A., Chaplain, M. A. J., Feb 2008. Mathematical modelling of cancer cell invasion of tissue: local and non-local models and the effect of adhesion. J Theor Biol 250 (4), 684–704.

Goldacre, R. J., Sylven, B., Jun 1962. On the access of blood-borne dyes to various tumour regions. Br J Cancer 16, 306–322.

Hanahan, D., Folkman, J., Aug 1996. Patterns and emerging mechanisms of the angiogenic switch during tumorigenesis. Cell 86 (3), 353–364.

Hogea, C. S., Murray, B. T., Sethian, J. A., Jul 2006. Simulating complex tumor dynamics from avascular to vascular growth using a general level-set method. J Math Biol 53 (1), 86–134.

Hu, B., Guo, P., Fang, Q., Tao, H.-Q., Wang, D., Nagane, M., Huang, H.-J. S., Gunji, Y., Nishikawa, R., Alitalo, K., Cavenee, W. K., Cheng, S.-Y., Jul 2003. Angiopoietin-2 induces human glioma invasion through the activation of matrix metalloprotease-2. Proc Natl Acad Sci U S A 100 (15), 8904–8909.

Kevrekidis, P. G., Whitaker, N., Good, D. J., Herring, G. J., Jun 2006. Minimal model for tumor angiogenesis. Phys Rev E Stat Nonlin Soft Matter Phys 73 (6 Pt 1), 061926.

Kim, Y.-M., Hwang, S., Kim, Y.-M., Pyun, B.-J., Kim, T.-Y., Lee, S.-T., Gho, Y. S., Kwon, Y.-G., Aug 2002. Endostatin blocks vascular endothelial growth factor-mediated signaling via direct interaction with kdr/flk-1. J Biol Chem 277 (31), 27872–27879.

Koga, K., Todaka, T., Morioka, M., Hamada, J., Kai, Y., Yano, S., Okamura, A., Takakura, N., Suda, T., Ushio, Y., Aug 2001. Expression of angiopoietin-2 in human glioma cells and its role for angiogenesis. Cancer Res 61 (16), 6248–6254.

Kumar, S., Weaver, V. M., Jun 2009. Mechanics, malignancy, and metastasis: the force journey of a tumor cell. Cancer Metastasis Rev 28 (1-2), 113–127.

Lee, D.-S., Rieger, H., Bartha, K., Feb 2006. Flow correlated percolation during vascular remodeling in growing tumors. Phys Rev Lett 96 (5), 058104.

Li, H.-L., Li, S., Shao, J.-Y., Lin, X.-B., Cao, Y., Jiang, W.-Q., Liu, R.-Y., Zhao, P., Zhu, X.-F., Zeng, M.-S., Guan, Z.-Z., Huang, W., Feb 2008. Pharmacokinetic and pharmacodynamic study of intratumoral injection of an adenovirus encoding endostatin in patients with advanced tumors. Gene Ther 15 (4), 247–256.

Lin, X., Huang, H., Li, S., Li, H., Li, Y., Cao, Y., Zhang, D., Xia, Y., Guo, Y., Huang, W., Jiang, W., May 2007. A phase 1 clinical trial of an adenovirus-mediated endostatin gene (e10a) in patients with solid tumors. Cancer Biol Ther 6 (5), 648–653.

Macklin, P., McDougall, S., Anderson, A. R. A., Chaplain, M. A. J., Cristini, V., Lowengrub, J., Apr 2009. Multiscale modelling and nonlinear simulation of vascular tumour growth. J Math Biol 58 (4-5), 765–798.

Maisonpierre, P. C., Suri, C., Jones, P. F., Bartunkova, S., Wiegand, S. J., Radziejewski, C., Compton, D., McClain, J., Aldrich, T. H., Papadopoulos, N., Daly, T. J., Davis, S., Sato, T. N.,

Yancopoulos, G. D., Jul 1997. Angiopoietin-2, a natural antagonist for tie2 that disrupts in vivo angiogenesis. Science 277 (5322), 55–60.

Mantzaris, N. V., Webb, S., Othmer, H. G., Aug 2004. Mathematical modeling of tumor-induced angiogenesis. J Math Biol 49 (2), 111–187.

McDougall, S. R., Anderson, A. R. A., Chaplain, M. A. J., Aug 2006. Mathematical modelling of dynamic adaptive tumour-induced angiogenesis: clinical implications and therapeutic targeting strategies. J Theor Biol 241 (3), 564–589.

Metheny-Barlow, L. J., Li, L. Y., Oct 2003. The enigmatic role of angiopoietin-1 in tumor angiogenesis. Cell Res 13 (5), 309–317.

Moon, W. S., Rhyu, K. H., Kang, M. J., Lee, D. G., Yu, H. C., Yeum, J. H., Koh, G. Y., Tarnawski, A. S., Jun 2003. Overexpression of vegf and angiopoietin 2: a key to high vascularity of hepatocellular carcinoma? Mod Pathol 16 (6), 552–557.

O'Reilly, M. S., Boehm, T., Shing, Y., Fukai, N., Vasios, G., Lane, W. S., Flynn, E., Birkhead, J. R., Olsen, B. R., Folkman, J., Jan 1997. Endostatin: an endogenous inhibitor of angiogenesis and tumor growth. Cell 88 (2), 277–285.

Partanen, J., Armstrong, E., Mäkelä, T. P., Korhonen, J., Sandberg, M., Renkonen, R., Knuutila, S., Huebner, K., Alitalo, K., Apr 1992. A novel endothelial cell surface receptor tyrosine kinase with extracellular epidermal growth factor homology domains. Mol Cell Biol 12 (4), 1698–1707.

Paweletz, N., Knierim, M., 1989. Tumor-related angiogenesis. Crit Rev Oncol Hematol 9 (3), 197–242.

Plank, M. J., Sleeman, B. D., Jones, P. F., Aug 2004. A mathematical model of tumour angiogenesis, regulated by vascular endothelial growth factor and the angiopoietins. J Theor Biol 229 (4), 435–454.

Pàez-Ribes, M., Allen, E., Hudock, J., Takeda, T., Okuyama, H., Viñals, F., Inoue, M., Bergers, G., Hanahan, D., Casanovas, O., Mar 2009. Antiangiogenic therapy elicits malignant progression of tumors to increased local invasion and distant metastasis. Cancer Cell 15 (3), 220–231.

Relf, M., LeJeune, S., Scott, P. A., Fox, S., Smith, K., Leek, R., Moghaddam, A., Whitehouse, R., Bicknell, R., Harris, A. L., Mar 1997. Expression of the angiogenic factors vascular endothelial cell growth factor, acidic and basic fibroblast growth factor, tumor growth factor beta-1, platelet-derived endothelial cell growth factor, placenta growth factor, and pleiotrophin in human primary breast cancer and its relation to angiogenesis. Cancer Res 57 (5), 963–969.

Ribba, B., Colin, T., Schnell, S., 2006a. A multiscale mathematical model of cancer, and its use in analyzing irradiation therapies. Theor Biol Med Model 3, 7.

Ribba, B., Marron, K., Agur, Z., Alarcón, T., Maini, P. K., Jan 2005. A mathematical model of doxorubicin treatment efficacy for non-hodgkin's lymphoma: investigation of the current protocol through theoretical modelling results. Bull Math Biol 67 (1), 79–99.

Ribba, B., Saut, O., Colin, T., Bresch, D., Grenier, E., Boissel, J. P., Dec 2006b. A multiscale mathematical model of avascular tumor growth to investigate the therapeutic benefit of anti-invasive agents. J Theor Biol 243 (4), 532–541.

Ribba, B., You, B., Tod, M., Girard, P., Tranchand, B., Trillet-Lenoir, V., Freyer, G., 2009. Chemotherapy may be delivered upon an integrated view of tumor dynamics. IET Systems Biology. Accepted.

Sauter, B. V., Martinet, O., Zhang, W. J., Mandeli, J., Woo, S. L., Apr 2000. Adenovirus-mediated gene transfer of endostatin in vivo results in high level of transgene expression and inhibition of tumor growth and metastases. Proc Natl Acad Sci U S A 97 (9), 4802–4807.

Sundberg, C., Kowanetz, M., Brown, L. F., Detmar, M., Dvorak, H. F., Apr 2002. Stable expression of angiopoietin-1 and other markers by cultured pericytes: phenotypic similarities to a subpopulation of cells in maturing vessels during later stages of angiogenesis in vivo. Lab Invest 82 (4), 387–401.

Takahashi, G. H., Fatt, I., Goldstick, T. K., Nov 1966. Oxygen consumption rate of tissue measured by a micropolarographic method. J Gen Physiol 50 (2), 317–335.

Tanaka, F., Ishikawa, S., Yanagihara, K., Miyahara, R., Kawano, Y., Li, M., Otake, Y., Wada, H., Dec 2002. Expression of angiopoietins and its clinical significance in non-small cell lung cancer. Cancer Res 62 (23), 7124–7129.

Tosin, A., Ambrosi, D., Preziosi, L., Oct 2006. Mechanics and chemotaxis in the morphogenesis of vascular networks. Bull Math Biol 68 (7), 1819–1836.

Welter, M., Bartha, K., Rieger, H., Jan 2008. Emergent vascular network inhomogeneities and resulting blood flow patterns in a growing tumor. J Theor Biol 250 (2), 257–280.

Zetter, B. R., 1998. Angiogenesis and tumor metastasis. Annu Rev Med 49, 407–424.

Zheng, X., Wise, S. M., Cristini, V., Mar 2005. Nonlinear simulation of tumor necrosis, neo-vascularization and tissue invasion via an adaptive finite-element/level-set method. Bull Math Biol 67 (2), 211–259.